

Venus's induced magnetosphere during active solar wind conditions at BepiColombo's Venus 1 flyby

Martin Volwerk¹, Beatriz Sánchez-Cano², Daniel Heyner³, Sae Aizawa⁴, Nicolas André⁴, Ali Varsani¹, Johannes Mieth³, Stefano Orsini¹⁰, Wolfgang Baumjohann¹, David Fischer¹, Yoshifumi Futaana⁹, Richard Harrison⁸, Harald Jeszenszky¹, Iwai Kazumasa⁵, Gunter Laky¹, Herbert Lichtenegger¹, Anna Milillo¹⁰, Yoshizumi Miyoshi⁵, Rumi Nakamura¹, Ferdinand Plaschke¹, Ingo Richter³, Sebastián Rojas Mata⁹, Yoshifumi Saito⁷, Daniel Schmid¹, Daikou Shiota⁶, and Cyril Simon Wedlund¹

¹Space Research Institute, Austrian Academy of Sciences, Graz, AT

²School of Physics and Astronomy, University of Leicester, Leicester, UK

³Institute for Geophysics and Extraterrestrial Physics, Technische Universität Braunschweig, DE

⁴IRAP, CNRS-UPS-CNRS, Toulouse, France

⁵Institute for Space-Earth Environmental Research, Nagoya University, Japan

⁶National Institute of Information and Communications Technology, Tokyo, Japan

⁷Institute of Space and Astronautical Science, Japan Aerospace Exploration Agency, Kanagawa, Japan

⁸RAL Space, UKRI-STFC Rutherford Appleton Laboratory, Harwell Campus, Oxfordshire, UK

⁹Swedish Institute of Space Physics, Kiruna, Sweden

¹⁰Institute of Space Astrophysics and Planetology, INAF, Rome, Italy

Correspondence: MARTIN VOLWERK (martin.volwerk@oeaw.ac.at)

Abstract. Out of the two Venus flybys that BepiColombo uses as a gravity assist manoeuvre to finally arrive at Mercury, the first took place on 15 October 2020. After passing the bow shock, the spacecraft travelled along the induced magnetotail, crossing it mainly in the Y_{VSO} -direction. In this paper, the BepiColombo Mercury Planetary Orbiter Magnetometer (MPO-MAG) data are discussed, with support from three other plasma instruments: the Planetary Ion Camera (SERENA-PICAM) of the SERENA

5 suite, the Mercury Electron Analyser (MEA) and the radiation monitor (BERM). Behind the bow shock crossing, the magnetic field showed a draping pattern consistent with field lines connected to the interplanetary magnetic field wrapping around the planet. This flyby showed a highly active magnetotail, with, e.g., strong flapping motions at a period of ~ 7 min. This activity was driven by solar wind conditions. Just before this flyby, Venus's induced magnetosphere was impacted by a stealth coronal mass ejection, of which the trailing side was still interacting with it during the flyby. This flyby is a unique opportunity to study 10 the full length and structure of the induced magnetotail of Venus, indicating that the tail was most likely still present at about 48 Venus radii.

Copyright statement. TEXT

1 Introduction

The interaction of Venus with the magnetoplasma of the solar wind gives rise to the creation of a so-called induced magnetosphere (see e.g., Luhmann et al., 1986; Phillips and McComas, 1991; Bertucci et al., 2011; Dubinin et al., 2011; Futaana et al., 2017). The solar wind is first braked by the upstream bow shock and is then further mass-loaded and slowed down due to the ionization of exospheric particles and their pick-up by the solar wind convection electric field, whilst approaching the planet. The magnetic field is subsequently draped around the planet (e.g. Saunders and Russell, 1986) in what is often called a comet-like interaction.

Closer to the planet the magnetic field piles up in a region that is known under various names: magnetic pile-up boundary, magnetic barrier or magnetopause (Zhang et al., 2008b, a). In this region, the interplanetary magnetic field (IMF) is stopped at the sunward side of the planet and cannot penetrate into the ionosphere. This boundary extends downstream to at least 11 planetary radii and encloses the induced magnetotail where planetary plasma escape mainly occurs (Bertucci et al., 2011). One more boundary is created through the difference in plasma composition, where there is a strong gradient in the energetic electrons and the ion population starts to become dominated by planetary ions instead of solar wind ions (Martinez et al., 2009a, b), the ion composition boundary. Finally, an additional boundary related to the upper limit of the collisional ionosphere is typically found at lower altitudes, the ionopause. This boundary is where the thermal ionospheric pressure balances the induced magnetosphere's magnetic pressure (Bertucci et al., 2011); it occurs mainly on the dayside and post-terminator nightside sectors.

In the dayside and upstream region of the induced magnetosphere various kinds of plasma waves are typically detected. In particular, two wave modes related to the pick-up of freshly created ions (Gary, 1992) in Venus's exosphere play an important role. In the solar wind, proton cyclotron waves are observed (Delva et al., 2008, 2015) created by the ion pick-up in a relatively low plasma- β environment. Behind the quasi-perpendicular bow shock, mirror-modes are often found (Volwerk et al., 2008a, b, 2016) because of the relatively high plasma- β there and the mainly perpendicular-to-the-magnetic-field energization of the ions crossing the bow shock.

In Venus's downstream region the induced magnetotail is created by the draped field lines, producing two regions of oppositely directed magnetic field separated by a current sheet (Phillips and McComas, 1991), not unlike the Earth's magnetotail. The direction of the field in the tail is mainly aligned with the direction of the solar wind and the field in the lobes is stronger than that in the magnetosheath (Russell et al., 1981). A difference in wave power between the magnetosheath and the tail proper can also be seen (Russell et al., 1981; Vörös et al., 2008a, b). As in the Earth's magnetotail, magnetic reconnection has been observed to take place (Volwerk et al., 2009, 2010; Zhang et al., 2010).

The first flythrough of Venus's magnetotail was done by Mariner 10 on 5 February 1974 (Lepping and Behannon, 1978), from as far downstream as $\sim 100 R_V$. In October 1975 the Venera 9 and 10 were injected into their very elongated orbits with pericentre at ~ 1500 km and apocentre at $\sim 110,000$ km and an inclination of 30° (Verigin et al., 1978; Eroshenko, 1979). The induced magnetosphere of Venus has only been studied over a limited region of space, because of the limited orbital coverage of the visiting spacecraft. Pioneer Venus Orbiter (PVO) did not explore the central region of the tail further than $\sim 11.5 R_V$

downstream of Venus, and Venus Express (VEX), due to a larger inclination of the spacecraft orbit, did not venture beyond $\sim 4 R_V$ downstream. This means that the structure and the dynamics of the Venusian far tail have not been fully characterised yet. Important questions are still open with respect to, e.g., the length of the tail and bow shock/wave along it: where does it 50 “merge” with the ambient solar wind? How do flux ropes and plasmoids move through the far tail? Learning this will have strong implications for understanding the processes that encourage the atmosphere to escape or shield it from doing so..

Recently, however, three newly launched missions have performed flybys using Venus as a gravitational assist to get into the correct orbit towards the inner solar system.

The first one was Parker Solar Probe (PSP, Fox et al., 2016), which is set to use 7 Venus flybys to adjust its perihelion 55 distance. The first flyby was on 3 October 2018, the second on 26 December 2019 approaching from the downstream direction, and the third on 11 July 2020, approaching from the upstream direction. The first flyby passed into the induced magnetosphere, where strong kinetic-scale turbulence was found in the magnetosheath (Bowen et al., 2021) as well as sub-proton scale magnetic holes (Goodrich et al., 2021), whereas the second flyby grazed Venus’s bow shock at the dawn terminator and double layers were observed at this boundary (Malaspina et al., 2020).

60 BepiColombo is the second new mission with two planned Venus flybys (Benkhoff et al., 2010; Milillo et al., 2020; Mangano et al., 2021), the first of which is the topic of this paper. The third mission is Solar Orbiter (Müller et al., 2013, 2020), which had its first Venus flyby about 2 months after the first BepiColombo flyby, on 27 December 2020.

This paper focuses on the first BepiColombo flyby that occurred on 15 October 2020. Since this flyby was the first opportunity to have scientific planetary observations after the instrumental tests performed during the Earth flyby on 10 April 2020, 65 several science instruments were turned on for this planetary encounter. The BepiColombo trajectory was such that by making a long transit into the Venusian induced magnetotail, it allowed for a precious opportunity to study the dynamics and structures of the tail, including the far tail, a region mostly unexplored.

2 The Data

The first BepiColombo flyby occurred on 15 October 2020 with closest approach at 03:58:31 UT and a minimum altitude of 70 10720.5 km above the planet surface (~ 2 Venus radii). BepiColombo was in the solar wind and crossed the Venusian bow shock on the day side in the evening sector, and then it did a long transit into the induced magnetotail. The flyby is shown in Fig. 1 in the Venus solar orbital (VSO) coordinate system. In this figure, the Sun is to the left ($+X_{VSO}$), and the different plasma boundaries together with BepiColombo’s trajectory are indicated.

The BepiColombo spacecraft (Anselmi and Scoon, 2001; Benkhoff et al., 2010) is still in its cruise phase configuration, 75 which means that there is a stacked formation: The Mercury Transfer Module (MTM), the Mercury Planetary Orbiter (MPO), the Magnetospheric Orbiter Sunshield and Interface Structure (MOSIF), and the Mercury Magnetospheric Orbiter (Mio). The main spacecraft MPO and MIO will first be detached at Mercury orbit insertion. Naturally, this formation brings limitations to the onboard instruments. With MIO behind the MOSIF heat shield many instruments will be obstructed (see below) and the

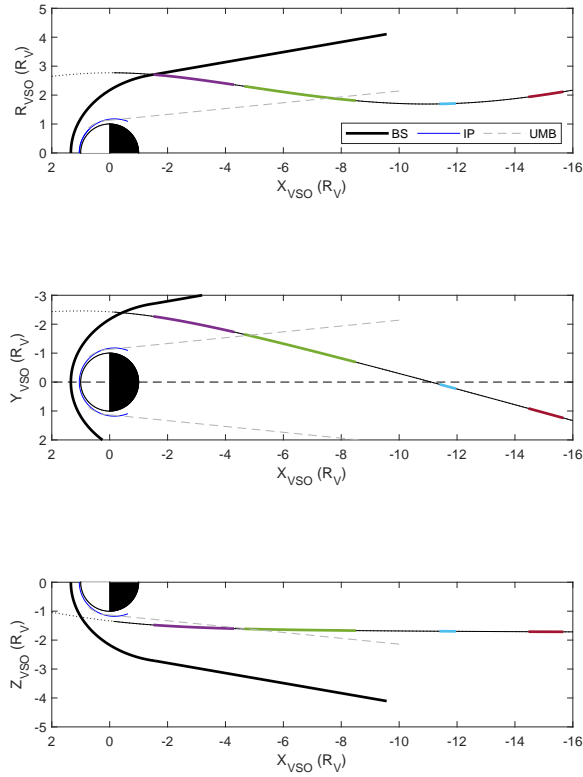


Figure 1. The BepiColombo first flyby to Venus in VSO coordinates (with $R_{\text{VSO}} = \sqrt{Y_{\text{VSO}}^2 + Z_{\text{VSO}}^2}$). The thick black line is the bow shock (BS) for solar minimum conditions (Zhang et al., 2008b), the thin blue line is the ionopause (IP) (Zhang et al., 2008b) and the grey dashed lines are the upper mantle boundary (UMB) (Martinez et al., 2009b). The thin black (dotted) line is the trajectory of BepiColombo, with the solid line showing the interval discussed in this paper. The purple, green, blue and red marked intervals are of special interest listed in Table 1

80 magnetometer boom cannot be deployed. For MPO the magnetometer boom could be deployed, however it is rather close to the MTM with its ion drives and solar panels, which will create stray fields in the measurements.

We use data from the BepiColombo magnetometer MPO-MAG on board the Mercury Planetary Orbiter (MPO) spacecraft (Glassmeier et al., 2010; Heyner et al., 2021), at a cadence of 1 second (Fig. 2) and a low-pass filter for periods below 5 minutes (Fig. 3) in order to get the large-scale structure of the induced magnetosphere undisturbed by high-frequency oscillations. We limit the discussion of the observations to the interval of 04:14 UT (crossing of the bow shock) to 12:00 UT, spanning the 85 region of $\sim 0 \geq X_{\text{VSO}} \geq -40 \text{ R}_V$ (Venus radius, $R_V = 6052 \text{ km}$).

This work focuses on different regions within the induced magnetosphere that are marked with purple-, green-, blue- and red-colours along the trajectory in Fig. 1.

In order to interpret the structure of the induced magnetosphere, the cone (θ_c) and clock (ϕ_c) angle of the magnetic field are calculated:

$$90 \quad \theta_c = \tan^{-1} \left(\frac{\sqrt{B_y^2 + B_z^2}}{B_x} \right), \quad (1)$$

$$\phi_c = \tan^{-1} \left(\frac{B_z}{B_y} \right). \quad (2)$$

These two angles describe the direction of the field: a cone angle of $\theta_c = 0^\circ/180^\circ$ indicates an sunward/anti-sunward direction and $\theta_c = 90^\circ$ indicates a field direction perpendicular to the Venus-Sun line. The clock angle shows the direction in the plane perpendicular to the Venus-Sun line with $\phi_c = 0^\circ/90^\circ$ indicating a field in the $Y_{\text{VSO}}/Z_{\text{VSO}}$ direction. In Fig. 3 the 95 magnetometer data are shown, as well as the cone and clock angles and the location of the spacecraft.

Data from Planetary Ion Camera (PICAM), part of the SERENA (Search for Exospheric Refilling and Emitted Natural Abundances) instrument suite (Orsini et al., 2010, 2021a, b), are also used to support the magnetometer data. PICAM is an ion mass spectrometer, which operates as an all-sky camera for charged particles. It is optimised for

Mercury's observations, to study the chain of processes by which neutrals are ejected from Mercury's soil, and are eventually 100 ionised and transported through the Hermean environment. PICAM operates by scanning through the energy and angular distribution of ions effectively from 10 eV up to 3 keV, and with a field of view of $1.5\pi \text{ sr}$ and a cadence of 64 s. PICAM also provides ion composition for a mass range extending up to $\sim 132 \text{ u}$ (Xenon).

Electron data from the Mercury Plasma Particle Experiment (Saito et al., 2010; Saito and et al., 2021) on board the Mercury Magnetospheric Orbiter (MMO, renamed Mio after launch) spacecraft of BepiColombo are also utilised. In particular, data 105 from the Mercury Electron Analyzer (MEA) 1 in solar wind mode (3 eV - 3000 eV) are used to investigate the low-energy electron distribution during the flyby at a cadence of 4 s. Since the MMO spacecraft is stuck behind the MOSIF sunshield during cruise phase, MEA1 has a limited field of view but, despite this, useful scientific observations can be obtained since low-energy electrons are almost isotropic.

In order to account for the solar wind activity responsible for the IMF disturbances around the Venus 1 flyby, data from the 110 BepiColombo Radiation Monitor (BERM) are used (Pinto et al., 2021). BERM is a particle detector able to provide radiation

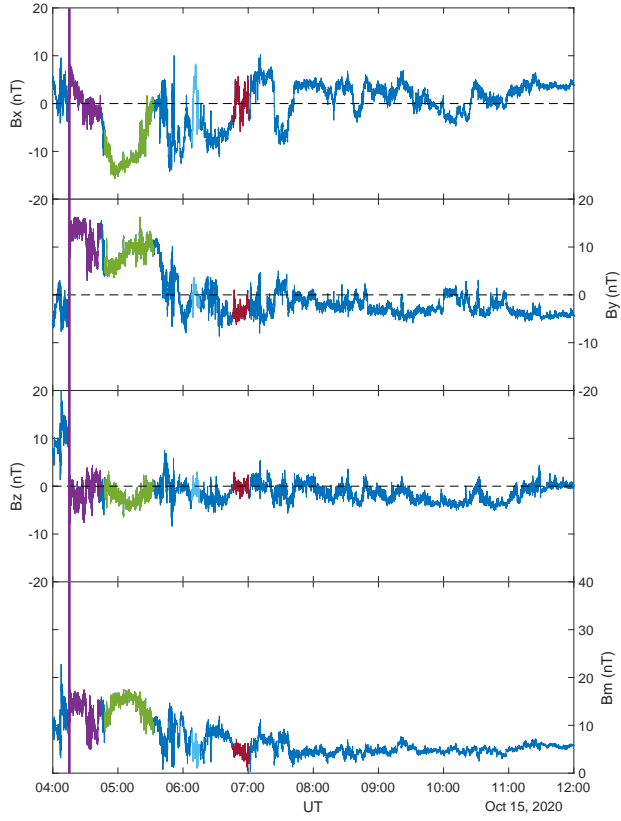


Figure 2. Full 1 s. resolution MPO-MAG data. Top to bottom panels show the B_x , B_y , B_z and the absolute magnetic (B_m) field components, respectively. The vertical purple line marks the bow shock transit. The purple, green, blue and red marked intervals are of special interest as in Fig. 1 and listed in Table 1

Table 1. Selected time intervals, based on the magnetometer data, showing different regions in Venus's induced magnetosphere behind the bow shock. The distance in the tail behind Venus in X_{VSO} is given in Venus radii, R_V .

| region | time in | time out | distance $ X_{\text{VSO}} $ | box colour |
|-------------------------|---------|-----------|-----------------------------|------------|
| bow shock & | | | | |
| magnetosheath | 04:14 | 04:44 | 1.5 – 4.2 | purple |
| magnetotail | 04:48 | 05:33 | 4.2 – 8.5 | green |
| around neutral sheet | 05:23 | 06:08 | 9.0 – 15.7 | NA |
| neutral sheet crossings | 06:08 | 06:15 | 11.3 – 12.0 | blue |
| flapping region | 06:46 | 07:01 | 14.5 – 15.7 | red |
| magnetotail | 07:45 | 14:00 (?) | 15.7 – 48 (?) | NA |

information, in a way similar to the Standard Radiation Environment Monitor (SREM) instrument aboard several ESA missions such as Rosetta (Honig et al., 2019). In particular, it is able to measure high-energy charged particles (e.g., electrons from \sim 100 keV to \sim 10 MeV and protons from 1 MeV to \sim 200 MeV), and the higher energy channels background counts can be used as a proxy for galactic cosmic rays.

115 Moreover, we also use data from the Large Angle and Spectrometric Coronagraph (LASCO) instrument on board the Solar and Heliospheric Observatory satellite (SOHO) (Brueckner et al., 1995). In particular, we use data from the c2 white light coronagraph imaging from 1.5 to 6 solar radii. We also use the Heliospheric Imager (HI) instrument, that forms part of the Sun Earth Connection Coronal and Heliospheric Investigation (SECCHI) suite of remote sensing instruments on board the Solar TErrestrial RElations Observatory (STEREO)-A spacecraft. The HI is a wide-angle visible-light imaging system for the 120 detection of coronal mass ejection (CME) events in interplanetary space covering the region of the heliosphere from 4 degrees to 88 degrees elongation measured from the Sun-centre (Howard et al., 2008; Eyles et al., 2009). It consists of two telescopes, HI1 and HI2: in this study we have used only images from HI1.

Finally, we have also used the Space-weather-forecast-Usable System Anchored by Numerical Operations and Observations (SUSANOO) model from Nagoya University to simulate the solar wind conditions encountered by BepiColombo at Venus during the flyby (Shiota et al., 2014; Shiota and Kataoka, 2016). SUSANOO is a magnetohydrodynamic (MHD) solar wind model of the inner heliosphere between 25 and 425 solar radii using a Yin-Yang grid, where the velocity, density and temperature are obtained from empirical models of the solar wind (Odstrčil and Pizzo, 1999a, b). CMEs are included in the inner boundary of the simulation as spheromak-type magnetic flux ropes (Shiota et al., 2014; Shiota and Kataoka, 2016; Iwai et al., 2019) with initial velocities derived semi-automatically from SOHO-LASCO.

130 In Fig. 3 there are four regions marked by differently coloured vertical lines, which will be discussed in more detail below. These intervals are also marked along the orbit of the flyby in Fig. 1. The times when these regions were transited and the distance to the planet when they occurred are listed in Table 1.

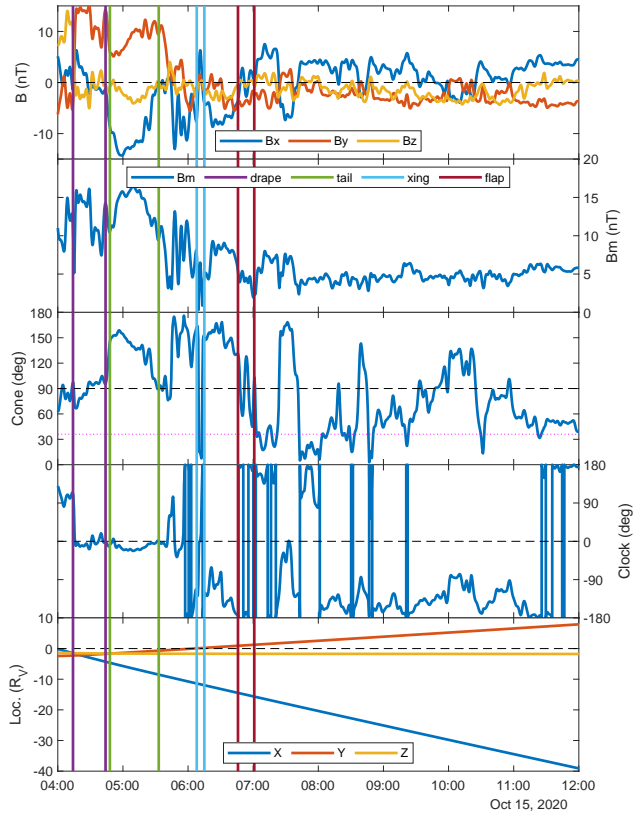


Figure 3. Magnetometer data in the magnetosheath and tail. From top to bottom: the three components of the magnetic field in VSO-coordinates; the magnitude of the magnetic field; the cone angle; the clock angle; and the location of the spacecraft in VSO-coordinates. The purple, green, blue and red dotted vertical lines show the intervals of interest.

3 MPO-MAG Observations

First the MPO-MAG data, based on the different regions as listed in Table 1 will be discussed.

135 3.1 Magnetosheath Draping

After crossing the bow shock at $\sim 04:14$ UT the spacecraft enters the Venusian magnetosheath. Fig. 4 shows a zoom-in on the field in the magnetosheath. It is clear that after the crossing of the bow shock (the first purple vertical line), the magnetic field rotates strongly from B_z (yellow) into B_y (red), which is also evident from the clock angle, ϕ_c , that turns from $\sim 90^\circ$ to $\sim 0^\circ$. B_x is the minor component in this interval, as can be clearly seen in the cone angle, $\theta_c \sim 90^\circ$.

140 This means that, in the magnetosheath, the magnetic field is mainly in the Y_{VSO} -direction, i.e., perpendicular to the induced magnetotail direction. This is reminiscent of the pattern described by Delva et al. (2017, their figure 1) where draped magnetic field lines in the magnetosheath were connected to the IMF, albeit that BepiColombo makes a much further excursion away from Venus, in this interval up to $X_{\text{VSO}} \approx -4R_V$, than VEX. This draping pattern was shown to exist in hybrid plasma simulations by Jarvinen et al. (2013).

145 3.2 Magnetotail Draping

After passing through the magnetosheath, there is a strong rotation of the magnetic field, at $\sim 04:44$ UT, where B_y decreases and B_x increases and the cone angle changes from $\theta_c \approx 90^\circ$ to $\approx 150^\circ$ as seen in Fig. 5 between the second purple and first green vertical line. Here, the magnetic field takes on the shape of a magnetotail, with the main direction along the Venus-Sun direction, albeit with a significant B_y contribution.

150 Because of the conic shape of the bow shock behind Venus, the magnetic field in the magnetosheath and magnetotail is not strictly along the Venus-Sun line, but flares out following this conic shape. A significant B_y contribution can be caused by this flaring of the magnetotail. However, we see in Fig. 5 that $B_x < 0$ and $B_Y > 0$, which is incompatible with flaring, for which one would expect $B_Y < 0$. This means that the “cross-tail magnetic field” B_y needs to have its origin elsewhere, e.g. from penetrating IMF into the tail. This can be caused via reconnection of the induced magnetic field with IMF structures. This 155 process is well known from Earth (e.g., Fairfield, 1979; Browett et al., 2017).

3.3 Neutral Sheet Crossing

At a bit further distances, BepiColombo encountered the neutral sheet. As can be seen in Fig. 5, at $\sim 05:25$ UT $|B_x|$ starts to decrease again ($B_x \rightarrow 0$ nT) and after $\sim 05:33$ UT B_y also starts to decrease, to end up at a minimum $B_m \approx 3$ nT around 160 05:43 UT, where then B_z is the dominant component for a short period of time, see Fig. 6. After 05:45 UT, there is a drastic change in the cone angle from $\sim 90^\circ$ to $\sim 180^\circ$ as well as large oscillations in B_x , B_m and in the clock angle that varies between ~ 180 and $\sim 0^\circ$. There are three of these oscillations, which then are followed by possible crossings of the neutral sheet between 06:08 and 06:15 UT. These neutral sheet crossings are marked by blue vertical lines in Fig. 6, and are seen as B_m reaching $\approx 0^\circ$ nT twice, and the cone angle varying from $\approx 150^\circ$ to $\approx 15^\circ$.

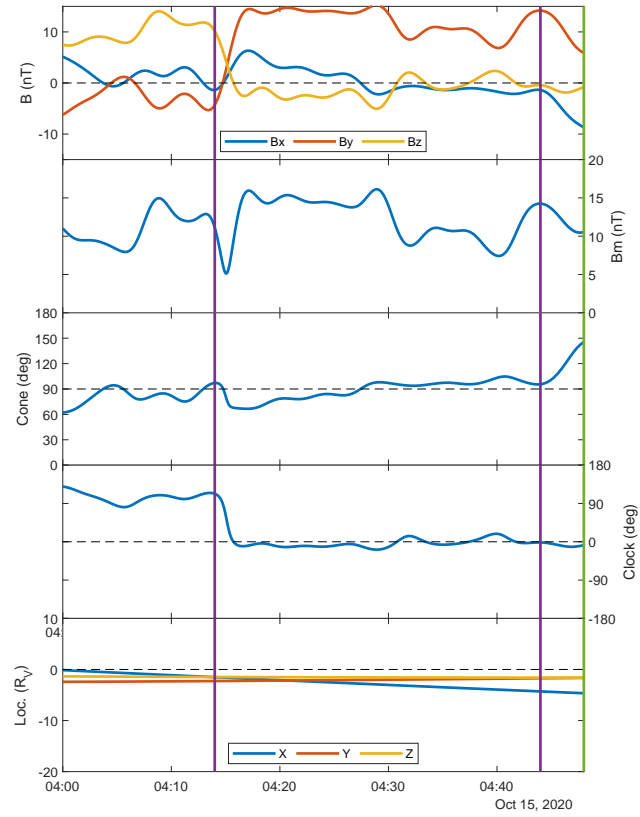


Figure 4. Zoom in on the magnetosheath interval (purple) where the cone angle $\theta_c \approx 90^\circ$ and the clock angle $\phi_c \approx 0^\circ$. This indicates that the magnetic field is pointing in the Y_{VSO} -direction.

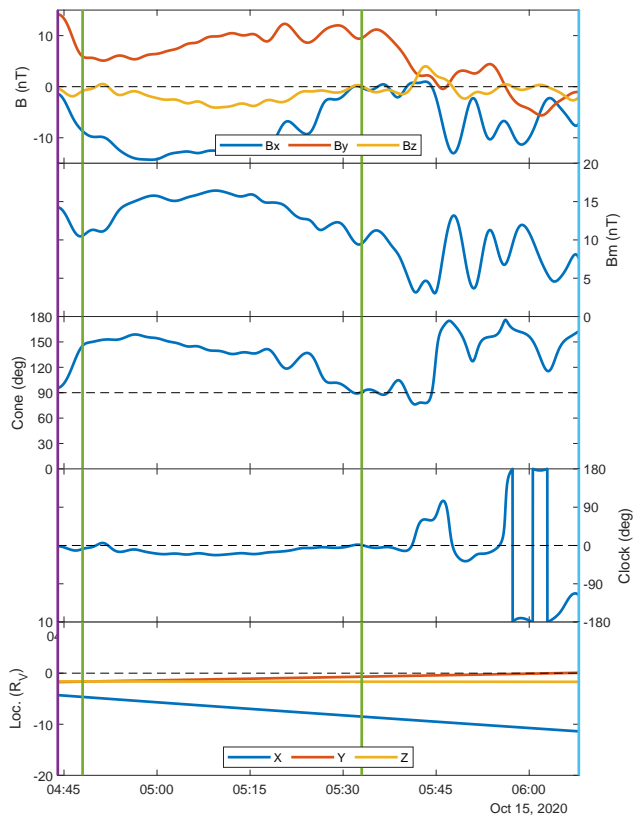


Figure 5. Zoom in on time interval (green) that BepiColombo is in the magnetotail proper. This interval shows a strongly draped field with $\theta_x \approx 150^\circ$, with a strong B_y component.

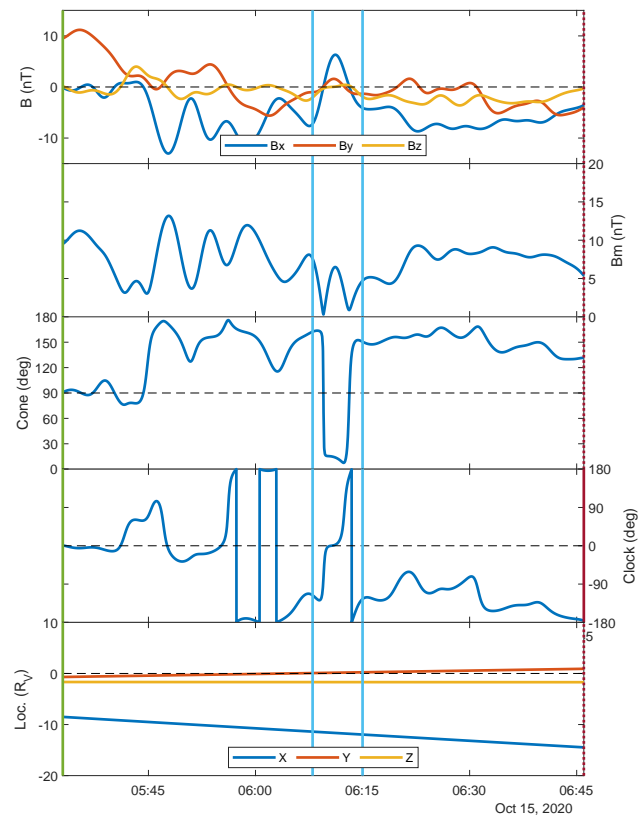


Figure 6. Zoom in on neutral sheet crossings interval (blue) Strong oscillations of the field also occur before the selected interval, without crossing $B_x = 0$ nT.

Table 2. Minimum variance direction for the $B_x = 0$ nT crossings (cr) rotated such that $n_x > 0$ and the eigenvalues of the MVA, where the ratio $\lambda_{\text{int}}/\lambda_{\text{min}}$ shows that the MVA is well determined.

| | cr1 | cr2 | cr3 | cr4 |
|---|--------------------|--------------------|--------------------|--------------------|
| start | 06:46 | 06:50 | 06:54 | 06:59 |
| end | 06:49 | 06:53 | 06:57 | 07:01 |
| n_x | 0.17 | 0.16 | 0.10 | 0.26 |
| n_y | 0.66 | 0.12 | 0.93 | 0.52 |
| n_z | -0.74 | -0.98 | 0.34 | -0.81 |
| λ_{min} | 1×10^{-4} | 2×10^{-5} | 1×10^{-3} | 1×10^{-4} |
| λ_{int} | 5×10^{-2} | 6×10^{-4} | 6×10^{-3} | 8×10^{-3} |
| λ_{max} | 3 | 3 | 3 | 1 |
| $\lambda_{\text{int}}/\lambda_{\text{min}}$ | 500 | 30 | 6 | 80 |

3.4 Magnetotail Flapping

165 Between 06:46 and 07:01 UT there are multiple crossings of $B_x = 0$ nT, with $B_y \approx -4$ nT and a negligible B_z (see Fig. 7). This behaviour is reminiscent of magnetotail flapping observed at Earth (Sergeev et al., 2003), and also evidenced in the Hermean magnetotail (Poh et al., 2020).

At Venus, this phenomenon has also been observed by Rong et al. (2015), with a period of ~ 3 min, which is much shorter than the ~ 7 min period seen in Fig. 7.

170 One of the characteristics of flapping is that for consecutive crossings of $B_x = 0$ nT the normal of the current sheet oscillates in the $Y - Z$ plane. We have performed a minimum variance analysis on the four crossings to determine the normal direction to the current sheet. The results are shown in Table 2. The determination of the direction normal to the current sheet appears robust, with eigenvalues well separated for each case and $\lambda_{\text{max}} \gg \lambda_{\text{int}} \gg \lambda_{\text{min}}$. As can be seen, the normal, $\mathbf{n} = (n_x, n_y, n_z)$, is mainly in the $Y - Z$ plane. For flapping, one would expect then that for $n_y > 0$ there is an alternately positive and negative 175 value for n_z . This is only the case for the last three crossings.

After these multiple crossings of $B_x = 0$ nT, there are two more excursions from one lobe to another, and then at $\sim 07 : 45$ UT the magnetic field strength basically arrives at a more-or-less constant value of $B_m \approx 5$ nT (see Fig. 3). The cone angle slowly rotates from $\theta_c \approx 20^\circ$ to $\theta_c \approx 140^\circ$ and then rotates back again, which is a characteristic as well of flapping activity within the tail. The flapping period is about 7 minutes.

180 **3.5 Exiting the bow shock**

As BepiColombo continues its path down and across the tail, it will eventually encounter the bow shock/wave again. It is not clear what this structure may look like so far down the tail, and thus from the magnetometer data it is difficult to determine where this crossing happened.

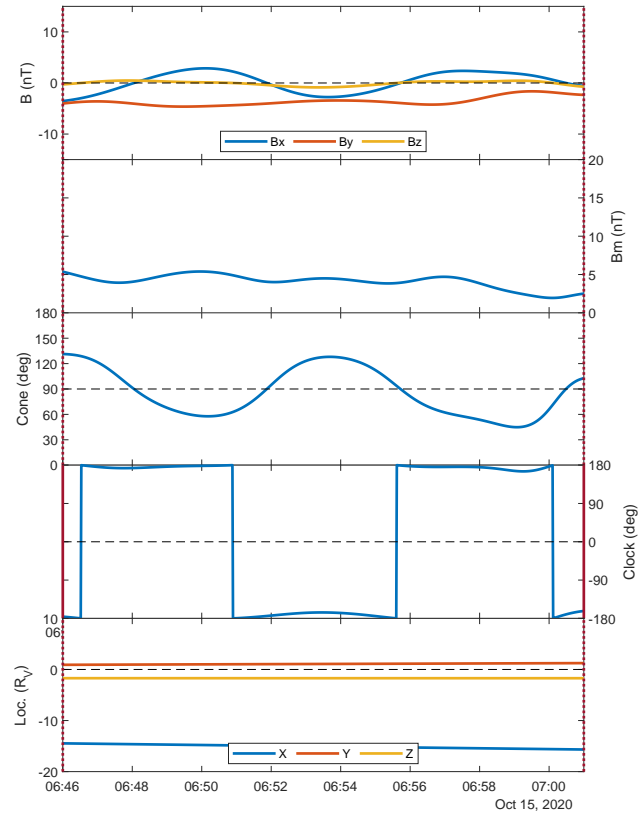


Figure 7. Zoom in on magnetotail flapping interval (red). The cone-angle clearly shows alternating magnetic field directions (tailward $\theta_c > 90^\circ$ and Venusward $\theta_c < 90^\circ$). The clock-angle remains basically the same ($\phi_c = 180^\circ \equiv \phi_c = -180^\circ$).

Table 3. The rotation of the cone angle for large excursions of BepiColombo in the lobes of Venus's magnetotail. The numbering of the crossings is shown in Fig. 8.

| Xing | 1-2 | 2-3 | 3-4 | 5-6 | 6-7 | 8-9 | 9-10 | 10-11 | 11-12 |
|------------------|------|------|------|-----|-----|-----|------|-------|-------|
| $\Delta\theta_c$ | 132° | 133° | 147° | 85° | 76° | 84° | 72° | 43° | 60° |

185 In order to get an estimate of where the crossing could have happened, we determine where the cone angle of the magnetic field varies around the average Parker-spiral angle of $\theta_P \approx 36^\circ$. This occurs around $\sim 14:00$ UT at a distance of $X_{VSO} \approx 48 R_V$ and $Y_{VSO} \approx 11 R_V$.

3.6 Magnetic Slingshot Effect

190 One phenomenon that may occur in the Venusian magnetotail is the so-called magnetic slingshot effect, where draped magnetic field lines, after they have slipped over/diffused through the ionosphere appear as kinked field lines in the tail. The kink represents a magnetic tension and ions will be accelerated by the $\mathbf{J} \times \mathbf{B}$ -force, as observed with PVO (Slavin et al., 1989).

Slowly, down the tail, the field line will “unkink,” which means that a spacecraft travelling down the tail, and moving alternately into the two lobes of the tail, e.g. through flapping motions, should see less rotation of the field. Slavin et al. (1989) showed that at a distance of $\sim 10 - 11 R_V$, the rotations of the field, when PVO crossed the central current sheet were close to $\Delta\phi \approx 180^\circ$, and associated with that accelerated H^+ and O^+ were observed.

195 With BepiColombo a very long trajectory through Venus's magnetotail was traversed. In Fig. 8 the low-pass filtered (periods longer than 30 minutes) cone angle is shown for 0400 - 2300 UT, corresponding to $X_{VSO} = 0 \dots - 94 R_V$. It was already determined above that the magnetotail is flapping, and in this case large oscillations of the cone angle are investigated, where the spacecraft moves from one lobe into the other. The extrema between the crossings of interest are labeled with numbers. The cone angle change is listed in Table 3. One can see that there is a small trend that the rotation $\Delta\theta_c$ decreases as the spacecraft 200 moves further down the tail. However, the orbit of BepiColombo was not optimal for such a study because of the large Z_{VSO} .

4 Plasma Data

4.1 BepiColombo

Fig. 9 shows PICAM, MPO-MAG and MEA1 observations. The PICAM data in Fig. 9 (first panel, which are as-yet uncalibrated, but with the background noise removed) show a strong signal of ~ 1 keV solar wind ions, both upstream of the bow 205 shock and inside the induced magnetotail. There are variations in the energy of the observed protons E_p , especially in the downstream region of the bow shock, between $\sim 04:45$ and $\sim 06:00$ UT with $6 \times 10^2 \leq E_p \leq 2 \times 10^3$ eV. Clear bursts of increased counts occur at the same time as an increase in the MEA electron counts is seen at energies between ~ 32 and ~ 100 eV. There are no measurements of the S/C potential, and therefore one caveat is that the energies for both electrons and

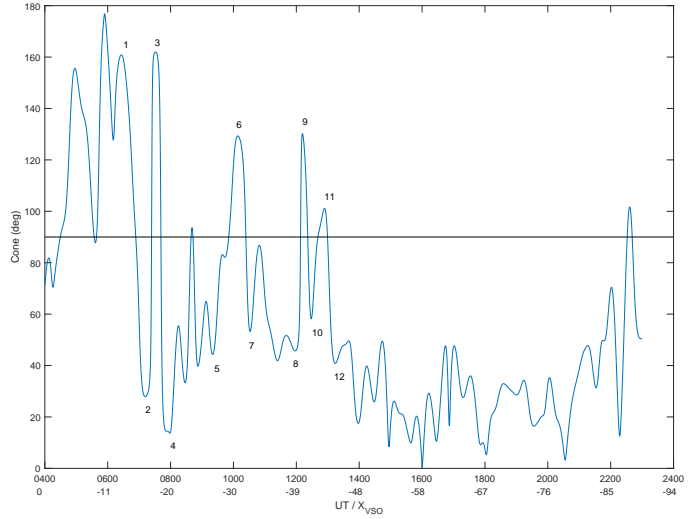


Figure 8. The cone-angle of the magnetic field calculated from low-pass filtered data, for periods longer than 30 minutes, for the interval 0400 - 2300 UT. The numbered peaks are used to calculate the change in cone-angle as BepiColombo moves from one lobe to the other, which is listed in Table 3. After 1400 UT the spacecraft is assumed to have left the magnetotail and to be in the solar wind.

ions might have some level of uncertainty. Nevertheless their trend should not be affected, as the timescale for changes in the 210 S/C potential is often much longer than the time interval of interest.

Interestingly, after crossing the bow shock, there is no clear reduction in the ion energy, which remains at solar wind level until $\sim 05:35$ UT. This is caused by the location of the bow shock crossing at $\sim [-1.5, -2.3, -1.5] R_V$, where the reduction of the plasma velocity is much smaller than towards the sub-solar point (see e.g., Spreiter et al., 1966; Spreiter and Stahara, 1994; Schmid et al., 2021). Overall, however, the counts decrease when BepiColombo moves further into the downstream region. 215 There are a few significant increases in the count rate, marked by grey and blue transparent boxes in Fig. 9. The grey boxes are when the spacecraft has entered the magnetotail, and there does not seem to be a good correlation between the PICAM and MPO-MAG data as far as these increases in counts is concerned. The first one is during a rotation of the field from B_x into B_y , the second shows no real peculiarities in the MPO-MAG data and the third shows a strong dip in B_x . The lack of one correlation between MPO-MAG and PICAM could be due to the FoV of PICAM which limits its visibility of the whole sky, 220 so that some ion jets might be missed in observations.

For the blue boxes, which occur during the period where the magnetic field is oscillating strongly, there seems to be a correlation between B_m and the PICAM count rate. The bursts of high counts correlate very well with the decreases in the total magnetic field.

Finally, during the interval labelled as “magnetotail flapping” (red-edged box) there is no increase in electron energy, but 225 there is a decrease in counts in the low-energy bins below 10 eV.

Table 4. A comparison of the boundary crossings determined from MEA and from MAG. There are two intervals for the plasma sheet for MAG, the second corresponds to the flapping interval.

| MEA | | crossing into/out of | MAG | |
|---------|----------|-------------------------|---------|-----------|
| time in | time out | | time in | time out |
| 04:08 | 13:04 | Bow Shock | 04:14 | 14:00 (?) |
| 04:53 | 07:37 | Induced Magnetosphere | 04:48 | 07:45 |
| 05:41 | 06:03 | Plasma Sheet | 05:43 | 06:15 |
| - | - | Plasma Sheet | 06:46 | 07:01 |

The MEA1 instrument was turned on from 14 October 2020 03:45:07 UT until 16 October 2020 04:25:51 UT. MEA1 measured low-energy electrons during the flyby except during wheel off-loading. The time-energy spectrogram of electron omnidirectional counts obtained every 4 seconds in the low-resolution telemetry mode is shown in Fig. 9, last panel. Table 4 shows the crossing times of the various regions as deduced from MEA1 data.. The times for some of the crossings are slightly off with respect to the magnetometer data (see also Table 1).

230

235

240

245

- The purple box is identified as the magnetosheath where the magnetic field was mainly in the Y_{VSO} -direction. The MEA data show after 04 : 08 UT a different population of electrons than that of the solar wind. The main population is at energies between 20 eV and 40 eV, with some variation to lower energies as the spacecraft moved deeper into the magnetosheath.
- The green box is identified as the magnetotail, where the cone angle is $\theta_c \approx 150^\circ$. In the MEA data this region shows a much broader distribution of electron energies between 3 eV and 40 eV. Between the purple and green box a magnetic field rotation takes place from $\theta_c \approx 90^\circ$ to $\theta_c \approx 150^\circ$. Already before the end of the purple box the electron energy distribution starts to broaden and reaches a maximum energy width at 04 : 53 UT, later than the rotation of the magnetic field. At the end of the green box, the spacecraft seems to move near the neutral sheet, with $B_m < 3$ nT, followed by strong oscillations in B_x and B_m . The MEA data show two electron populations, one at 3 – 10 eV and one at 30 – 80 eV. This splitting of the electron population can be caused by acceleration through the electric field generated by the magnetic field gradients.
- The blue box shows the actual crossing of a neutral sheet, with $B_m \approx 0$ nT. Interestingly, there is no signature in the MEA data here, just a broad energy distribution of the electrons.
- The red box is the location of the “magnetotail flapping”, the multiple crossings of $B_x = 0$ nT. The MEA data show a decrease in the low-energy electron population.

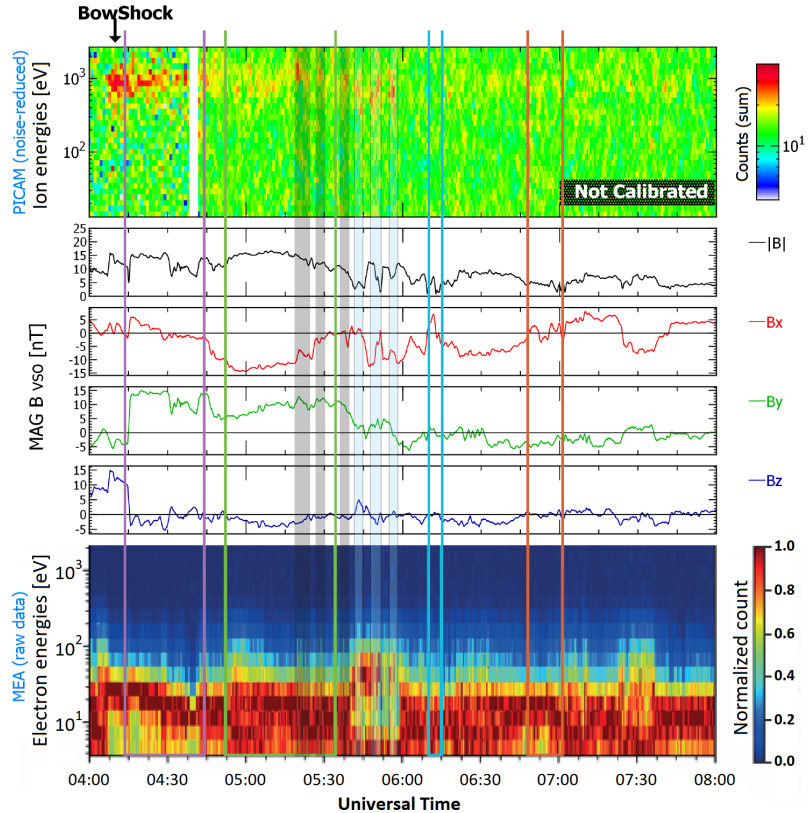


Figure 9. Four hours of the Venus 1 flyby as seen by different instruments. Top panel shows the PICAM data, where the ~ 1 keV protons are clearly visible before and behind the bow shock. The data gap near $\sim 04:40$ UT is caused by a mode change. The middle four panels show the MAG data, B-field magnitude and components. The bottom panel shows the linearly normalized MEA omnidirectional electron count time-energy spectrogram. The coloured lines (purple, green, cyan and red) and the shaded areas (transparent grey, transparent blue) show the different intervals as defined in the text.

4.2 Comparison to a Venus Express magnetotail flapping event and ICME interaction

Venus Express (VEX, Svedhem et al., 2007) also observed magnetotail flapping in the near-Venus tail around $(-1.5, 0.1, 0.5) R_V$ on 24 November 2007, as shown in Fig. 10, discussed by Rong et al. (2015). These authors stated that, different from the Earth's magnetotail where the source for flapping is expected at the centre (Sergeev et al., 2003; Davey et al., 2012), the source for the flapping in Venus's tail is located near the boundaries between magnetotail current sheet and magnetosheath.

The second and third panels show the magnetometer data (Zhang et al., 2006) $B_{x,y,z}$ and B_m . The first and fourth panels show the Analyser of Space Plasma and Energetic Atoms, ASPERA-4 IMA ion mass composition sensor derived proton differential flux at a time resolution of 12 s and the ASPERA-4 ELS electron sensor derived electron differential flux time-

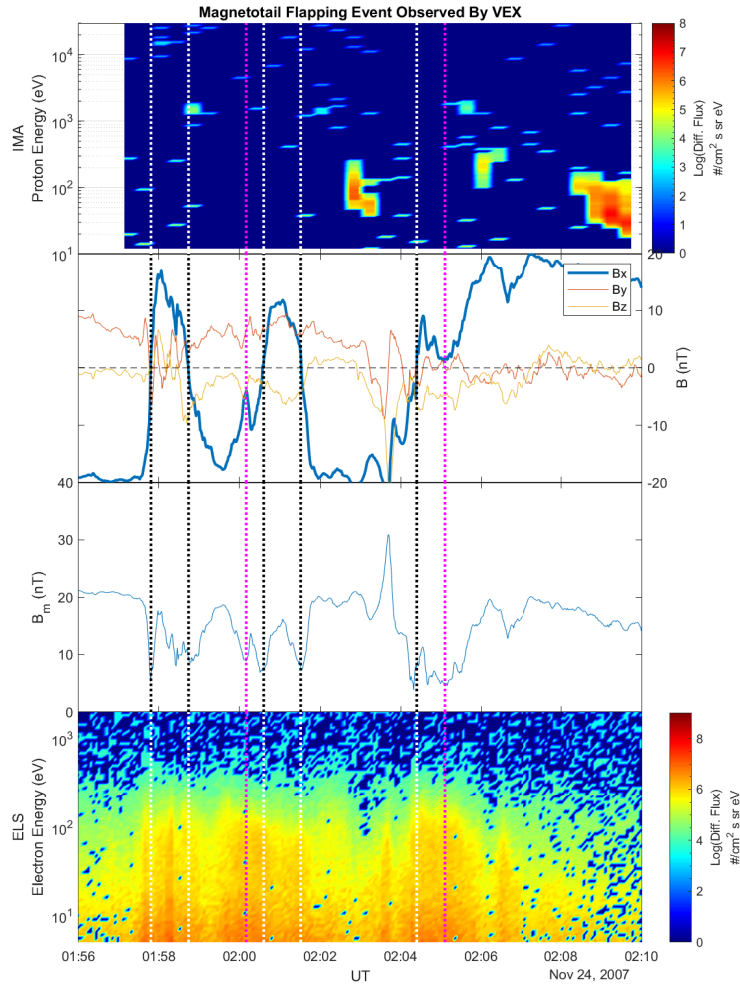


Figure 10. Magnetotail flapping event at Venus in the near-tail (near $\sim (-1.5, 0.1, 0.5)$) observed by Venus Express on 24 November 2007 (see also Rong et al., 2015). The top panel shows the proton differential flux time-energy spectrogram. The second panel shows the three components of the magnetic field. B_x is in a thick blue line showing how it oscillates over the spacecraft moving VEX from one lobe to the other. The third panel shows B_m with clear dips when $B_x = 0$ nT. The bottom panel shows the electron differential flux time-energy spectrogram. The white/black vertical dotted lines show the $B_x = 0$ nT crossings, where magenta lines show times when B_x approaches but does not reach 0 nT

255 energy spectrogram at a time resolution of 4 s (Barabash et al., 2007). The black (white) vertical dotted lines show where $B_x = 0$ nT, the two magenta vertical dotted lines show where VEX approaches $B_x = 0$ nT, but does not cross over.

260 The IMA time-energy spectrogram shows some weak bursts at $\gtrsim 1$ keV (most likely solar wind protons). At lower energies, protons between ~ 20 and ~ 200 eV, there are three bursts in the time-energy spectrogram. These seem to be correlated with VEX being in the lobes of the magnetotail, at $|B_x| \approx 20$ nT. This is different from what was observed by BepiColombo, where the PICAM bursts seemed to be correlated with minimal observed magnetic field strength.

265 The ELS spectrogram shows that when the spacecraft approaches the centre of the tail, the flux at higher energies increases (near the vertical lines in Fig. 10) indicating that there are more energetic electrons in the central plasma sheet of Venus's induced magnetotail. Note that the flux is strongly reduced when VEX is in the lobes, whenever $|B_x|$ increases, indicating that the energetic electrons are a feature of the central plasma sheet.

270 There are, however, clear differences between the flapping events as observed by BepiColombo and VEX. First of all, the flapping amplitude is about twice as large for VEX. Secondly, in the blue boxes in Fig. 9, where we see the splitting of the electron populations, there are no $B_x = 0$ nT crossings, so BepiColombo remains in one lobe of the induced magnetotail. Later, in the red box, BepiColombo does cross $B_x = 0$ nT multiple times.

275 Comparing the electron energy distribution for MEA1 and ELS for the blue boxes in Fig. 9 and Fig. 10 one can see that for ELS there is no splitting of the electron population into two energy bands. Also ELS does not show a drop in flux at the $B_x = 0$ nT crossing as is observed in the MEA1 data in the red box.

Naturally, these differences may well be caused by the difference in location of the spacecraft with VEX near $X \approx -1.5R_V$ and BepiColombo near $X \approx -15R_V$, as well as the different spacecraft speeds and instrument cadences.

280 Dimmock et al. (2018) studied the interaction of an ICME with the Venusian induced magnetosphere, both with numerical simulations and VEX observations. They showed that the magnetic environment around Venus can be strongly altered, albeit mainly on the dayside, through bringing the bow shock more planetward, increasing the field strength at the magnetic barrier, up to a value of ~ 270 nT, and magnetizing the ionosphere. The field line draping pattern was similar to "regular" conditions, although the simulation did not match the night-side draping pattern very well. The VEX data showed that there were large amplitude oscillations in front of and behind the bow shock, which are assumed to be whistler waves. Magnetotail dynamics are, unfortunately, not discussed.

4.3 Mariner 10, Galileo and Pioneer Venus

285 As Mariner 10 was on its way to Mercury, it passed through Venus's magnetotail (wake) on 5 February 1974, in a similar orbit in the $X - R$ -plane as BepiColombo, but at positive Z (see, Lepping and Behannon, 1978). The wake magnetic field data were studied starting at a distance of $\sim 100R_V$ from the planet. No evidence was found for a bow shock crossing entering the far tail. No typical magnetotail structure (as compared to Earth) was observed, but the authors found that, when the magnetic field direction and the spacecraft velocity vector aligned, the direction was not predominantly along X_{VSO} , as one would expect for a magnetotail along the orbit of Mariner 10.

The data were categorized into three bins, quiet, disturbed and mixed. The longitudinal (cylindrical) component of the field was observed to rotate clockwise, when the spacecraft crossed from a quiet to a disturbed region. Lepping and Behannon 290 (1978) interpreted this as Mariner 10 entering into planetary magnetotail, however, with a significant Y -component for most crossings. The IMF, after Mariner 10 crossed the bow shock, exiting the induced magnetosphere was $F = 20$ nT (in the paper denoted as 20γ), $\phi \approx 360^\circ$ and $\theta \approx 0^\circ$ (Ness et al., 1974). This means a mostly radial magnetic field. These multiple crossings do not seem to happen for BepiColombo. During the Solar Orbiter flyby such crossings were observed (Volwerk et al., 2021).

The Galileo spacecraft used a Venus gravitational assist on its way to Jupiter. During this Venus flyby, the orbit skimmed 295 the bow shock. Kivelson et al. (see e.g., 1991) used the magnetometer data to investigate the cross section of the bow shock. They found that it seemed to be smaller when its direction was aligned with the IMF when compared to when its direction was perpendicular to the IMF.

Using Pioneer Venus data, Slavin et al. (1989) studied Venus's near-tail region, at $|X| \lesssim 12 R_V$. Twelve passes through the 300 central induced magnetotail (in the period 1981 – 1983) along Pioneer Venus's polar orbit were studied, and it was found that the spacecraft traversed the central current sheet multiple times during each crossing. The quasi-period of the crossings is $\lesssim 10$ min (as estimated from their figures). The spacecraft moved between clearly defined oppositely directed fields. This behaviour could be considered magnetotail flapping, however, this was not yet a named phenomenon.

The main difference between the BepiColombo passage through Venus's tail and the orbits studied by Slavin et al. (1989) is the IMF direction. For BepiColombo the IMF is mainly in the Z -direction, whereas for the Pioneer Venus events the IMF 305 is mainly in the Y -direction. This means that the morphology of the induced magnetotail is rather different. For the Pioneer Venus orbits the central current sheet was almost in the $X - Z$ -plane d, whereas for BepiColombo the central current sheet is almost in the $X - Z$ -plane.

5 Solar Wind Interaction: Context for Venus's magnetotail observations

5.1 BepiColombo Solar Wind Conditions

310 Many of the features seen in the magnetometer data are in good agreement with what one would expect for draped magnetic field lines from the solar wind inducing a magnetosphere around Venus. However, it is also clear that the solar wind was disturbed based on the significant activity of the tail such as the multiple neutral sheet crossings and flapping of the tail.

In a pre-flyby study, McKenna-Lawlor et al. (2018) discussed the space weather near Venus during the BepiColombo flybys, where one could expect interactions with, e.g., Interplanetary Coronal Mass Ejections (ICMEs) and Corotating Interaction 315 Regions (CIRs). However, during the actual BepiColombo flyby 1 our interpretation of the solar wind interaction with the induced magnetosphere is hampered by the lack of an upstream solar wind monitor. Nevertheless, thanks to pre- and post-flyby observations made by the MPO-MAG, BERM and MEA1 instruments, together with observations made by STEREO-A, SOHO and a solar wind numerical simulation, the space weather context of the encounter is reconstructed.

Fig. 11 shows some STEREO and SOHO observations of a potential CME that may have hit Venus during the BepiColombo 320 flyby. The Space Weather Database Of Notifications, Knowledge, Information (DONKI) catalogue reports a single CME event

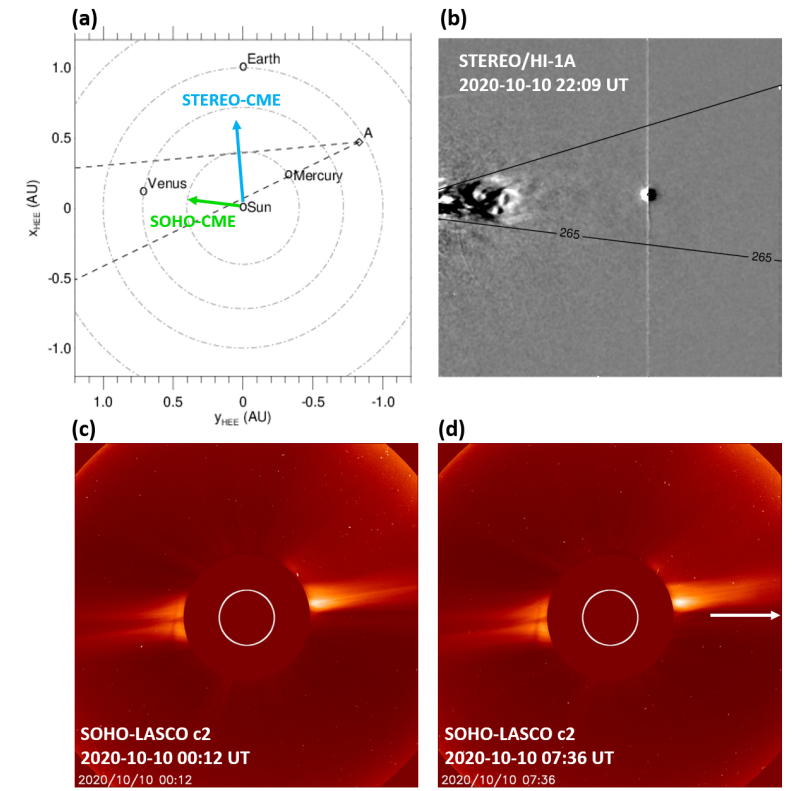


Figure 11. STEREO and SOHO observations. (a) Planet and STEREO A (A) positions and elongation range of the field-of-view in the plane of the sky of STEREO-A/HI1 (this is a 20 degree angle in the two dimensions). The blue and green arrows indicates the direction of the nose of the CMEs seen by SOHO and STEREO nearly simultaneously. (b) STEREO-A/HI1 image in a running difference format (where, in each case, the previous image is subtracted from the current image to highlight changes). The most northern and southern position angles of the CME spans are plotted as black lines and Venus is the bright dot towards the center. (c and d) SOHO-LASCO c2 images before and during the CME transit, respectively. The white arrow indicates the plasma motion off the west limb, which is more evident at the movie created at the SOHO Movie Theater (<https://soho.nascom.nasa.gov/data/Theater/>).

for the period 7-13 October, which corresponds to the time needed for a CME to reach Venus by the time of the BepiColombo flyby. The DONKI catalogue indicates that this event was observed by SOHO-LASCO c2, c3 and STEREO-A SECCHI instruments with a starting time on 10 October 2020 04:24 UT and a speed of 270.0 km/s. This specific DONKI run also lists a direction right on the western limb (with respect to Earth). Moreover, no clear source eruption (filaments or prominence activity) in the Solar Dynamic Observatory (SDO) imagery was observed. This event is clearly seen by the SOHO-LASCO instrument in panels c and d, where plasma outflows along a west limb streamer seen from L1 go into Venus's direction (Venus was near in quadrature with respect to Earth, see panel a).

325 However, the Heliospheric Cataloguing, Analysis and Techniques Service (HELCATS), which provides the official interplanetary CME catalogue of the STEREO HI instruments, reveals a rather different scenario. HELCATS (Harrison et al., 2018) 330 catalogues the derivation of CME kinematic properties (direction, speed and launch time) from geometric fitting techniques applied to the HI observations, described in Davies et al. (2013). The technique applies a Self Similar Expansion (SSE) approach that assumes a circular CME topology, expanding within two fixed position angles. The validity of this assumption depends on the nature of the particular event under study and the derived parameters should be regarded as best estimates in the spirit of that assumption. For the event under study (Figure 10), the SSE fit suggests that the HI-observed CME was a weak CME 335 ejected by the Sun on 9 October at 23:05 UT with a speed of 283 km/s. The first observation of the CME by the HI1 camera was on 10 October at 10:09UT and the fit indicates that it was near Earth-directed. No clear arrival was detected in the vicinity of Earth, though the solar wind parameters do show some signs of disturbance, though, of course, the CME might have simply passed near to the Earth. However, overall, we conclude that there is some evidence that the near simultaneous weak CMEs 340 observed by both STEREO-A and SOHO were not the same, that is, we witness a near-Earth directed CME from the STEREO instrumentation and coincident CME activity associated with a streamer with the SOHO data, that is directed towards Venus. The SOHO-observed CME could well have hit BepiColombo at the time of its first flyby to Venus.

In order to estimate the arrival time of this CME at Venus, Fig. 12 shows the main outputs of a SUSANOO simulation. Panels a-c show three stills of the solar wind velocity in the ecliptic plane. For completeness, the simulation has also included the following CME observed by SOHO-LASCO, that was ejected on 13 October 2020 at 21:12 UT with close direction to 345 Venus as well. Panels d-e show the same simulation in a 3D view. Finally, panel f shows the IMF (magnitude), the density, and the velocity of the solar wind temporal variation. The arrival and ending time of the CME transits at BepiColombo is indicated with vertical dashed lines in panel f. According to the simulation, the CME arrived at BepiColombo and Venus on 13 October 2020 at about noon (UT time). Since the velocity was relatively low, it needed a couple of days to transit Venus. The simulation predicts that the CME left Venus on 15 October 2020 at about 15 UT. Therefore, the BepiColombo flyby most 350 probably occurred while the CME was still transiting Venus. The second CME most probably also hit Venus after the flyby arriving on 17 October 2020 as predicted by the simulation.

Figure 13 shows the actual solar wind observations made by BepiColombo from 12 to 17 October. In particular, it shows: the IMF measured by the MPO-MAG in panel (a), the proxy for galactic cosmic ray flux measured by BERM in panel (b), and the solar wind energetic electron spectra from MEA1 in panel (c). The reason for the large data gaps in panel (c) is that 355 MEA1 only operated for a few hours around the closest approach. This figure corroborates that the solar wind was indeed

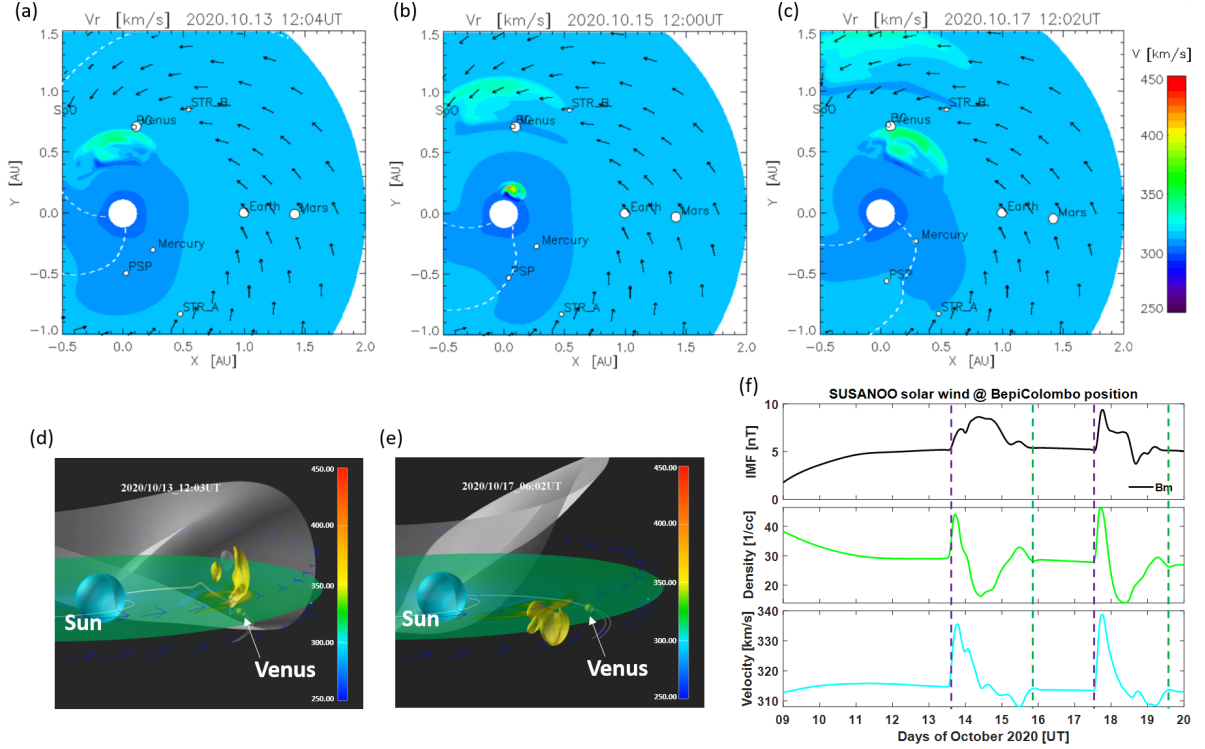


Figure 12. Stills from the SUSANOO simulation performed for the period 9–18 October 2020. (a–c) 2D plots of the solar wind velocity at the ecliptic plane on 13 October 2020 at 12:04 UT (CME arrival at BepiColombo), 15 October 2020 at 12:00 UT (trailing edge of the CME leaves BepiColombo), and 17 October 2020 at 12:02 UT (a second CME arrival at BepiColombo). The Sun is the white largest circle, the different planets and satellites are also labelled and the black arrows show the direction of the solar wind flow. The yellowish blobs toward Venus represent the CMEs of this study. The background colours represent the speed, as indicated in the colour scale. (d–e) Same as before but in 3D. The green plane is the ecliptic and the white-transparent surface is the heliospheric current sheet. The yellowish blobs toward Venus are the CMEs of this study. The colorbar velocity is only applicable to the CME. (f) Time series of IMF (magnitude in black), density (in green) and velocity (in light blue) at the BepiColombo location obtained from the simulation. The vertical dashed purple and green lines indicate the arrival and end time of the CMEs at BepiColombo.

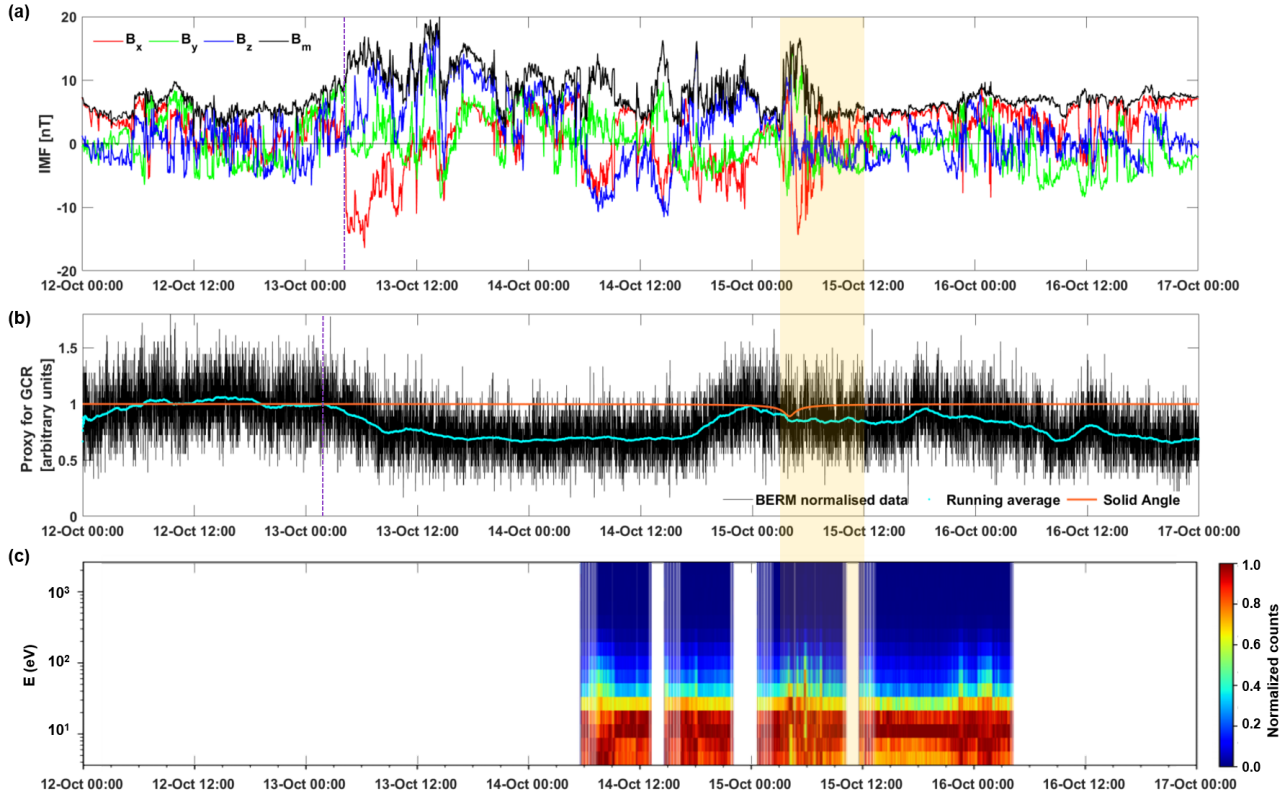


Figure 13. Solar wind observations: (a) Magnetic field observations from MPO-MAG in VSO, (b) Proxy for Galactic Cosmic Rays (GCR) observations from BERM and part of the BepiColombo solid angle not shadowed by Venus, (c) energy electron spectrograms from MEA1. The arrival time of the coronal mass ejection (CME) is marked with a vertical purple dashed line and the Venus transit (same period of the observations of this paper) is marked with a yellowish box.

clearly disturbed. The overall magnitude of the solar wind is ~ 15 nT for most of the period, similar to the induced magnetic field values observed at Venus (yellowish box). The CME arrived at BepiColombo on 13 October at 04:20 UT (vertical purple dashed line), where a moderate rise in the IMF magnitude from 10 to 15 nT was observed simultaneously with a rotation in the three components of the field, mainly seen in B_x . Moreover, starting a few hours before, a significant reduction in the Galactic

360 Cosmic Ray (GCR) flux was observed (purple dashed line in panel b) and the GCR flux remained low for almost 2 days. These kinds of reductions followed by a gradual recovery could be associated with Forbush decreases, which are produced by the magnetic flux rope inside the CME that scatters away the incoming GCR (Witasse et al., 2017). In this sense, Forbush decreases are good indicators of CME arrivals. The IMF magnitude was maintained at ~ 15 nT and the level of GCR was kept relatively constant until few hours before the encounter with Venus. MEA1 observations also agree with the idea of a CME transiting 365 as the variability observed in the solar wind energetic electron observations matches very well with the magnetic variability, especially when the B_x and B_z components are negative. This corroborates the idea that the solar wind was disturbed just

a few hours before BepiColombo's Venus encounter. These small and slow CMEs are transients often seen during low solar activity phases of the solar cycle and are often called stealth-CMEs because, as in this case, no clear source is identified. BepiColombo has already encountered several transient structures of this type, such as that presented in Heyner et al. (2021). 370 Although stealth-CMEs typically are pushed by the solar wind, they have the capacity of interacting with planet's conductive surface and ionosphere plasma: this is especially the case for unmagnetised planets as demonstrated in this study at Venus and also with similar events at Mars by Sánchez-Cano et al. (2017) and Kajdič et al. (2021). In addition, we also note that during 375 the closest approach (starting and ending right before and after the Venus inbound and outbound, respectively), the radiation monitor BERM detected a moderate reduction of 12% in the GCR flux proxy. The reason for this reduction is unknown and could be consequence of a solid angle effect from Venus, similar to those observed at Mars at an orbiter periapsis (e.g. Semkova et al., 2018). For this reason, panel (b) shows the part of the BepiColombo's solid angle not shadowed by Venus in orange, where 1 stands for null shadowed (null solid angle). The solid angle has been calculated as $\omega = 2\pi(1 - \cos\theta)$, where theta is the linear angle between the BepiColombo's distance to the center of the planet and the BepiColombo's distance to the limb of 380 the planet, which in turn is calculated as the arcsine of the ratio between the Venus' radius and the BepiColombo's distance to the center of the planet. The part of space not shadowed by the solid angle (orange line) is calculated as $1 - (\omega/4\pi)$. We note that the BERM flux level reduction that can be attributed to the solid angle effect lasts much shorter than the actual nearly constant reduction found. Nevertheless, other effects more difficult to discern may be also playing a role, such as shadowing from the own spacecraft due to attitude changes. Interestingly, Rosetta also saw a similar reduction in the GCR flux of 8% in 385 the vicinity of the comet 67P/Churyumov-Gerasimenko which could not be attributed to any known mechanisms (Honig et al., 2019).

Right after the flyby, there was still significant solar wind variability and according to the simulation in Fig. 12, these perturbations are most probably caused by the trailing edge of the CME. This means that during the flyby to Venus, the system was most probably immersed in the CME. The MEA1 observations also corroborate this finding showing a large perturbation 390 in the solar wind electrons on 15 October at 22:00 UT at the same time that a large variability is observed on the MPO-MAG data with B_x and B_z IMF rotations.

5.2 Venus Express Solar Wind Conditions

Interestingly, Kajdič et al. (2021) noticed that in November 2007 there was a good alignment of Mercury, Venus, Earth and Mars. In the period of 20 to 27 November, during the presented VEX event, a CME and two stream interaction regions (SIRs) were observed by ACE, STEREO A and B, and Mars Express. With the aforementioned alignment of the planets it stands to 395 reason that Venus's induced magnetosphere was also impacted by these structures.

This means that the solar wind conditions during the VEX event, shown in Fig. 10, are very comparable with those during the BepiColombo flyby. Even though VEX traversed the tail much closer to the planet, the disturbance of the magnetosphere through an outside source is clear through the flapping motion, driven from outside-in (Rong et al., 2015).

6 Conclusions

400 The first Venus encounter by BepiColombo has shown a new view of the Venusian induced magnetosphere up to about 48 Venus radii downstream. Until this flyby only one spacecraft had ever ventured this far down the magnetotail, Mariner 10 (Lepping and Behannon, 1978). A few months later, in December 2020, Solar Orbiter also had its Venus flyby over a similar distance along the tail investigating its dynamics (see e.g. Fig. 14 and Volwerk et al., 2021).

405 The asymmetric draping of the magnetic field, just behind the bow shock in the magnetosheath, as observed by Delva et al. (2017) and modelled by Jarvinen et al. (2013), was confirmed by this flyby. The field pointed in the direction perpendicular to the Venus-Sun line before the spacecraft entered the magnetotail proper.

410 The magnetotail was very active, with strong oscillations of the magnetic field with $\Delta B/B \approx 0.6$, with a period of ~ 7 min. This oscillation or flapping of the magnetotail was slower than what was typically measured by VEX in 2007, where Rong et al. (2015) determined a period of ~ 3 min. However, observations in the Earth's magnetotail show that the magnetotail flapping period varies from ~ 3 min. (Sergeev et al., 2003) to ~ 20 min. (Zhang et al., 2005).

415 During the strong oscillations of the magnetic field SERENA-PICAM measured increased ion fluxes when the total field was at a minimum. At the same time MEA showed that there were two populations of electrons, one below 10 eV and one between 32 and 100 eV. The latter "hot" population was also observed by Venus Express much closer to the planet.

420 Despite the low solar activity conditions, the flyby was affected by the impact of a stealth coronal mass ejection that was travelling at approximately the same speed than the background solar wind and impacted Venus and BepiColombo about 2 days before the closest approach on 13 October. Due to the low speed of this CME, in-situ magnetic and particle observations together with a solar wind simulation indicate that the trailing part of the CME was still affecting Venus at the time of the BepiColombo's closest approach and tail transit. A second CME may have hit both Venus and BepiColombo on 17 October, in principle, not affecting the flyby. Therefore, the highly dynamic tail observed by BepiColombo may be the consequence of space weather activity.

425 On 10 August 2021, the second Venus flyby will take place, where BepiColombo will approach the planet from the tail side, and pass closely by the planet in the dayside magnetosphere, as shown in Fig. 14 bottom panel. One day earlier, on 9 August, Solar Orbiter will also have its second Venus flyby in a more similar orbit as the first flyby. This means that both spacecraft can act as solar wind monitors for the other mission, during these flybys. This will be an unprecedented occasion to obtain two-point global measurements around Venus.

Data availability. The BepiColombo MPO-MAG, PICAM, MEA and BERM data, as well as the Venus Express MAG and ASPERA-4 data are available through ESA's Planetary Science Archive (PSA, <https://archives.esac.esa.int/psa>). The STEREO data are available through the HELCATS catalogue (https://www.helcats-fp7.eu/catalogues/event_page.html). The SOHO data are available through NASA's SOHO website (<https://soho.nascom.nasa.gov/data/Theater/>).

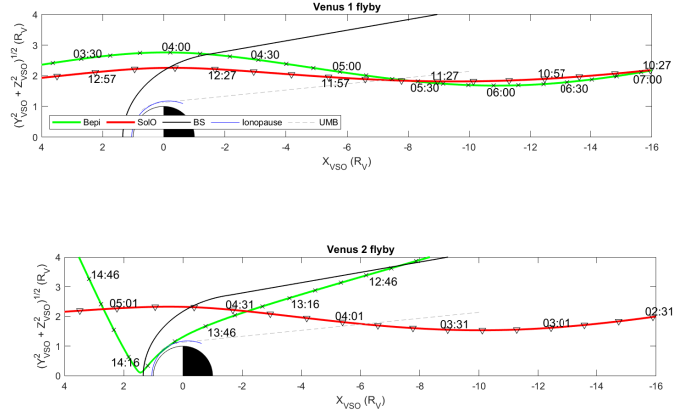


Figure 14. A comparison of the first and second Venus flybys by BepiColombo (green) and Solar Orbiter (red). Venus 1 flyby was on 15 October 2020 for BepiColombo and on 27 December for Solar Orbiter. The Venus 2 flybys will take place on 9 August 2021 for Solar Orbiter and on 10 August for BepiColombo.

430 *Author contributions.* M.V., B.S.-C. and D.H. instigated the MPO-MAG data investigation. J.M. and I.R. calibrated the MPO-MAG data. S.A. and N.A. provided the MEA data and interpretation. A.V., H.J. and G.L. provided the PICAM data and interpretation. Y.M., I.K., D.S. and Y.S. provided the SUSANOO simulations. R.H. provided the STEREO data and interpretation. F.P., D.S., C.S.W., R.N. and W.B. helped with interpreting the results. S.R.M. and Y.F provided the Venus Express ASPERA-4 data.

Competing interests. The authors have no competing interests.

435 *Acknowledgements.* Based on observations obtained with BepiColombo, a joint ESA - JAXA science mission with instruments and contributions directly funded by ESA Member States and JAXA. B.S.-C. acknowledges support through UK-STFC grants ST/S000429/1 and ST/V000209/1. C.S.W. is supported by the Austrian Science Fund (FWF) under project P32035-N36. D.H. was supported by the German Ministerium für Wirtschaft und Energie and the German Zentrum für Luft- und Raumfahrt under contract 50 QW 1501. N.A. and S.A. acknowledge the support of CNES for the BepiColombo mission. MEA data analysis was performed with the CL software developed by
440 Emmanuel Penou at IRAP and the AMDA science analysis system provided by the Centre de Données de la Physique des Plasmas (CDPP) supported by CNRS, CNES, Observatoire de Paris and Université Paul Sabatier, Toulouse. D.S. and D.F. work is financially supported by the Austrian Research Promotion Agency (FFG) ASAP MERMAG-4 under contract 865967. S.R.M. was funded by the Swedish National Space Agency under contracts 79/19 and 145/19.

References

445 Anselmi, A. and Scoon, G. E. N. (2001), 'Bepicolombo, ESA's Mercury cornerstone mission', *Planet. Space Sci.* **49**, 1409 – 1420.

Barabash, S., Sauvaud, J.-A., Gunell, H., Andersson, H., Grigoriev, A., Brinkfeldt, K., Holmström, M., Lundin, R., Yamauchi, M., Asamura, K., Baumjohann, W., Zhang, T., Coates, A., Linder, D., Kataria, D., Curtis, C., Hsieh, K., Sandel, B., Fedorov, A., Mazelle, C., Thocaven, J.-J., Grande, M., Koskinen, H. E., Kallio, E., Säles, T., Riihela, P., Kozyra, J., Krupp, N., Woch, J., Luhmann, J., McKenna-Lawlor, S., Orsini, S., Cerulli-Irelli, R., Mura, M., Milillo, M., Maggi, M., Roelof, E., Brandt, P., Russell, C., Szego, K., Winningham, J., Frahm, R.,
450 Scherrer, J., Sharber, J., Wurz, P. and Bochsler, P. (2007), 'The analyser of space plasmas and energetic atoms (ASPERA-4) for the Venus Express mission', *Planet. Space Sci.* **55**, 1772 – 1792.

Benkhoff, J., Casteren, J., Hayakawa, H., Fujimoto, M., Laakso, H., Novara, M., Ferri, P., Middleton, H. R. and Ziethe, R. (2010), 'Bepi-
colombo comprehensive exploration of Mercury: Mission overview and science goals', *Planet. Space Sci.* **58**, 2 – 20.

Bertucci, C., Duru, F., Edberg, N., Fraenz, M., Martinecz, C., Szego, K. and Vaisberg, O. (2011), 'The induced magnetospheres of Mars,
455 Venus, and Titan', *Space Sci Rev* **162**, 113–171.

Bowen, T. A., Bale, S. D., Bandyopadhyay, R., Bonnell, J., Case, A., Chasapis, A., Chen, C. H. K., Curry, S., Dudok de Wit, T., Goetz, K.,
Goodrich, K., Gruesbeck, J., Halekas, J., Harvey, P. R., Howes, G. G., Kasper, J., Korreck, K., Larson, D., Livi, R., MacDowall, R. J.,
Malaspina, D. M., Mallet, A., McManus, M., Page, B., Pulupa, M., Raouafi, N., Stevens, M. and Whittlesey, P. (2021), 'Kinetic-scale
turbulence in the Venusian magnetosheath', *Geophys. Res. Lett.* p. in press.

460 Browett, S. D., Fear, R. C., Grocott, A. and Milan, S. E. (2017), 'Timescales for the penetration of IMF By into the Earth's magnetotail', *J. Geophys. Res.* **122**, 579 – 593.

Brueckner, G., Howard, R., Koomen, M., Korendyke, C. M., Michels, D. J., Moses, J. D., Socker, D. G., Dere, K. P., Lamy, P. L., Llebaria,
A., Bout, M. V., Schwenn, R., Simnett, G. M., Bedford, D. K. and Eyles, C. J. (1995), 'The large angle spectroscopic coronagraph (lasco)',
Sol Phys **162**, 357–402.

465 Davey, E. A., Lester, M., Milan, S. E. and Fear, R. C. (2012), 'Storm and substorm effects on magnetotail current sheet motion', *J. Geophys. Res.* **117**, A02202.

Davies, J. A., Harrison, R. A., Perry, C. H., Möstl, C., Lugaz, N., Rollett, T., Davis, C. J., Crothers, S. R., Temmer, M. and Eyles, C. J. (2012),
'A self-similar expansion model for use in solar wind transient propagation studies', *Astrophys. J.* **750**, 23.

Davies, J. A., Perry, C. H., Trines, R. M. G. M., Harrison, R. A., Lugaz, N., Möstl, C., Liu, Y. D. and Steed, K. (2013), 'Establishing a
470 stereoscopic technique for determining the kinematic properties of solar wind transients based on a generalized self-similarly expanding
circular geometry', *The Astrophysical Journal* **777**, 167.

Delva, M., Bertucci, C., Volwerk, M., Lundin, R., Mazelle, C. and Romanelli, N. (2015), 'Upstream proton cyclotron waves at Venus near
solar maximum', *J. Geophys. Res.* **120**, 344 – 354.

Delva, M., Volwerk, M., Jarvinen, R. and Bertucci, C. (2017), 'Asymmetries in the magnetosheath field draping on Venus' nightside', *J.
475 Geophys. Res.* **122**, 10396 – 10407.

Delva, M., Zhang, T. L., Volwerk, M., Vörös, Z. and Pope, S. A. (2008), 'Proton cyclotron waves in the solar wind at Venus', *Geophys. Res. Lett.* **113**, E00B06.

Dimmock, A. P., Alho, M., Kallio, E., Pope, S. A., Zhang, T. L., Kilpua, E., Pulkkinen, T. I., Futaana, Y. and Coates, A. J. (2018), 'The
response of teh Venus plasma environment to the passage of an ICME: Hybrid simulation results and Venus Express observations', *J.
480 Geophys. Res.* **123**, 3580 – 3601.

Dubinin, E., Fraenz, M., Fedorov, A., Lundin, R., Edberg, N., Duru, F. and Vaisberg, O. (2011), 'Ion energization and escape on Mars and Venus', *Space Sci. Rev.* **162**, 173 – 211.

Eroshenko, E. G. (1979), 'Unipolar induction effects in the magnetic tail of Venus', *Cosmic Res.* **17**, 93 – 105.

Eyles, C., Harrison, R. and Davis, C. e. a. (2009), 'he heliospheric imagers onboard the stereo mission', *Sol Phys* **254**, 387–445.

485 Fairfield, D. H. (1979), 'On the average configuraton of the geomagnetic tail', *J. Geophys. Res.* **84**, 1950 – 1958.

Fox, N. J., Velli, M. C., Bale, S. D., Decker, R., Driesman, A., Howard, R. A., Kasper, J. C., Kinnison, J., Kusterer, M., Lario, D., Lockwood, M. K., McComas, D. J., Raouafi, N. E. and Szabo, Z. (2016), 'The Solar Probe Plus mission: Humanity's first visit to our star', *Space Sci. Rev.* **204**, 7 – 48.

Futaana, Y., Stenberg Wieser, G., Barabash, S. and Luhmann, J. G. (2017), 'Solar wind interaction and impact on the venus atmosphere',
490 *Space Sci. Rev.* **212**, 1543 – 1509.

Gary, S. P. (1992), 'The mirror and ion cyclotron anisotropy instabilities', *J. Geophys. Res.* **97**, 8519 – 8529.

Glassmeier, K. H., Auster, H. U., Heyner, D., Okrafska, K., Carr, C., Berghofer, G., Anderson, B. J., Balogh, A., Baumjohann, W., Cargill, P., Christensen, U., Delva, M., Dougherty, M., Fornaçon, K. H., Horbury, T. S., Lucek, E. A., Magnes, W., Mandea, M., Matsuoka, A., Matsushima, M., Motschmann, U., Nakamura, R., Narita, Y., O'Brien, H., Richter, I., Schwingenschuh, K., Shibuya, H., Slavin, J. A.,
495 Sotin, C., Stoll, B., Tsunakawa, H., Vennerstrom, S., Vogt, J. and T.L.Zhang (2010), 'The fluxgate magnetometer of the BepiColombo Mercury Planetary Orbiter', *Planet. Space Sci.* **58**, 287 – 299.

Goodrich, K. A., Bonnell, J. W., Curry, S., Livi, R., Whittlesey1, P., Mozer, F., Malaspina3, D., Halekas4, J., McManus, M., Bale, S., Bowen, T., Case, A., Dudok de Wit, T., Goetz, K., Harvey, P., Kasper, J., Larson, D., MacDowall, R., Pulupa, M. and Stevens, M. (2021), 'Evidence of sub-proton-scale magnetic holes in the Venusian magnetosheath', *Geophys. Res. Lett.* p. Submitted.

500 Harrison, R. A., Davies, J. A., Barnes, D., Byrne, J. P., Perry, C. H., Bothmer, V., Eastwood, J. P., Gallagher, P. T., Kilpua, E. K. J., Möstl, C., Rodriguez, Rouillard, A. P. and Odstrčil, D. (2018), 'CMEs in the heliosphere: I. A statistical analysis of the observational properties of CMEs detected in the heliosphere from 2007 to 2017 by STEREO/HI-1', *Sol. Phys.* **293**, 77.

Heyner, D., Auster, H.-U., Fornacon, K.-H., Carr, C., Richter, I., Mieth, J. Z. D., Kolhey, P., Exner, W., Motschmann, U., Baumjohann, W., Matsuoka, A., Magnes, W., Berhofer, G., Fischer, D., Plaschke, F., Nakamura, R., Narita, Y., Delva, M., Volwerk, M., Balogh, A.,
505 Dougherty, M., Horbury, T., lanlais, B., Mandea, M., Masters, A., Oliveira, J. S., Sánchez-Cano, B., Slavin, J. A., Vennerstrøm, S., Vogt, J., Wicht, J. and Glassmeier, K.-H. (2021), 'The BepiColombo planetary magnetometer MPO-MAG: What can we learn from the Hermean magnetic field?', doi:10.1007/s11214-021-00822-x, *Space Sci. Rev.* **217**, 52.

Honig, T., Witasse, O. G., Evans, H., Nieminen, P., Kuulkers, E., Taylor, M. G. G. T., Heber, B., Guo, J. and Sánchez-Cano, B. (2019), 'Multi-point galactic cosmic ray measurements between 1 and 4.5 au over a full solar cycle', *Ann. Geophys.* **37**, 903–918.

510 Howard, R. A., Moses, J. D., Vourlidas, A., Newmark, J., Socker, D. G., Plunkett, S. P., Korendyke, C. M., Cook, J. W., Hurley, A., Davila, J. M., Thompson, W. T., St Cyr, O. C., Mentzell, E., Mehalick, K., Lemen, J. R., Wuelser, J. P., Duncan, D. W., Tarbell, T. D., Wolfson, C. J., Moore, A., Harrison, R. A., Waltham, N. R., Lang, J., Davis, C. J., Eyles, C. J., Mapson-Menard, H., Simnett, G. M., Halain, J. P., Defise, J. M., Mazy, E., Rochus, P., Mercier, R., Ravet, M. F., Delmotte, F., Auchere, F., Delaboudiniere, J. P., Bothmer, V., Deutsch, W., Wang, D., Rich, N., Cooper, S., Stephens, V., Maahs, G., Baugh, R., McMullin, D. and Carter, T. (2008), 'Sun earth connection coronal and heliospheric investigation (SECCHI)', *Space Sci. Rev.* **136**, 67 – 115.

Iwai, K., Shiota, D., Tokumaru, M., Fujiki, K., Den, M. and Kubo, Y. (2019), 'Development of a coronal mass ejection arrival time forecasting system using interplanetary scintillation observations', *Earth Planets Space* **71**, 39.

Jarvinen, R., Kallio, E. and Dyadechkin, S. (2013), ‘Hemispheric asymmetries of the Venus plasma environment’, *J. Geophys. Res.* **118**, 4551 – 4563.

520 Kajdič, P., Sánchez-Cano, B., Neves-Ribeiro, L., Witasse, O., Bernal, G. C., Rojas-Castillo, D., Nilsson, H. and Fedorov, A. (2021), ‘Interaction of space weather phenomena with mars plasma environment during solar minimum 23/24’, *J. Geophys. Res.* **126**, e2020JA028442.

Kivelson, M. G., Kennel, C. F., McPherron, R. L., Southwood, D. J., Walker, R. J., Hammond, C. M., Khurana, K. K., Strangeway, R. J. and Coleman, P. J. (1991), ‘Magnetic Field Studies of the Solar Wind Interaction with Venus from the Galileo Flyby’, *Science* **253**, 1518 – 1522

525 Lepping, R. P. and Behannon, K. W. (1978), ‘Mariner 10 magnetic field observations of the Venus wake’, *J. Geophys. Res.* **83**, 3709 – 3720.

Luhmann, J. G., Russell, C. T. and Elphic, R. C. (1986), ‘Spatial distributions of magnetic field fluctuations in the dayside magnetosheath’, *J. Geophys. Res.* **91**, 1711 – 1715.

530 Malaspina, D. M., Goodrich, K., Livi, R., Halekas, J., McManus, M., Curry, S., Bale, S. D., Bonnell, J. W., Dudok de Wit, T., Goetz, K., Harvey, P. F., MacDowall, R. J., Pulupa, M., Case, A. W., Kasper, J., Korreck, K. E., Larson, D., Stevens, M. L. and Whittlesey, P. (2020), ‘Plasma double layers at the boundary between Venus and the Solar wind’, *Geophys. Res. Lett.* **47**, e2020GL090115.

535 Mangano, V., Dósa, M., Fränz, M., Milillo, A., Lee, J. S. O. Y. J., McKenna-Lawlor, S., Grassi, D., Heyner, D., Kozyrev, A. S., Peron, R., Helbert, J., Besse, S., de la Fuente, S., Montagnon, E., Zender, J., Volwerk, M., Chaufray, J., Slavin, J. A., Krüger, H., Maturilli, A., Cornet, T., Iwai, K., Miyoshi, Y., Lucente, M., Massetti, S., Schmidt, C. A., Dong, C., Quarati, F., Hirai, T., Varsani, A., Belyaev, D., Zhong, J., Kilpua, E. K. J., Jackson, B. V., Odstrcil, D., Plaschke, F., Vainio, R., Jarvinen, R., Lambrov Ivanovski, S., Madár, A., Erdös, G., Plainaki, C., Alberti, T., Aizawa, S., Benkhoff, J., Murakami, G., Quemerais, E., Hiesinger, H., Mitrofanov, I. G., Iess, Santoli, F., Orsini, S., Lichtenegger, H., Laky, G., Barabash, S., Moissl, R., Huovelin, J., Kasaba, Y., Saito, Y., Kobayashi, M. and Baumjohann, W. (2021), ‘Bepicolombo science investigations during cruise and flybys at the Earth, Venus and Mercury’, *Space Sci. Rev.* **217**, 23.

540 Martinecz, C., Boesswetter, A., Fränz, M., Roussos, E., Woch, J., Krupp, N., Dubinin, E., Motschmann, U., Wiede, S., Simon, S., Barabash, S., Lundin, R., Zhang, T. L., Lammer, H., Lichtenegger, H. and Kulikov, Y. (2009a), ‘Correction to ‘Plasma environment of Venus: Comparison of Venus Express ASPERA-4 measurements with 3-D hybrid simulations’’, *J. Geophys. Res.* **114**, E00B98.

Martinecz, C., Boesswetter, A., Fränz, M., Roussos, E., Woch, J., Krupp, N., Dubinin, E., Motschmann, U., Wiede, S., Simon, S., Barabash, S., Lundin, R., Zhang, T. L., Lammer, H., Lichtenegger, H. and Kulikov, Y. (2009b), ‘Plasma environment of Venus: Comparison of Venus Express ASPERA-4 measurements with 3-D hybrid simulations’, *J. Geophys. Res.* **114**, E00B30.

545 McKenna-Lawlor, S., Jackson, B. and Odstrcil, D. (2018), ‘Space weather at planet Venus during the forthcoming BepiColombo flybys’, *Planet. Space Sci.* **152**, 176 – 185.

Milillo, A., Fujimoto, M., Murakami, G., Benkhoff, J., Zender, J., Dósa, S. A. M., Griton, L., Heyner, D., Ho, G., Imber, S., Jia, X., Karlsson, T., Killen, R., Laurenza, M., Lindsay, S., McKenna-Lawlor, S., Mura, A., Raines, J., Rothery, D., André, N., Baumjohann, W., Berezhnoy, A., Bourdin, P., Bunce, E., Califano, F., Deca, J., de la Fuente, S., Dong, C., Grava, C., Fatemi, S., Henri, P., Ivanovski, S., Jackson, B., James, M., Kallio, E., Kasaba, Y., Kilpua, E., Kobayashi, M., Langlais, B., Leblanc, F., Lhotka, C., Mangano, V., Martindale, A., Massetti, S., Masters, A., Morooka, M., Narita, Y., Oliveira, J., Odstrcil, D., Orsini, S., Pelizzo, M., Plainaki, C., Plaschke, F., Sahraoui, F., Seki, K., Slavin, J., Vainio, R., Wurz, P., Barabash, S., Carr, C., Delcourt, D., Glassmeier, K.-H., Grande, M., Hirahara, M., Huovelin, J., Koralev, O., Kojima, H., Lichtenegger, H., Livia, S., Matsuoka, A., Moiss, R., Moncuquet, M., Muinonen, K., Quemerais, E., Saito, Y., Yagitani, S., Yoshikawa, I. and Wahlund, J.-E. (2020), ‘Investigating Mercury’s environment with the two-spacecraft BepiColombo mission’, *Space Sci. Rev.* **216**, 93.

555 Müller, D., Marsden, R. G., St. Cyr, O. C., Gilbert, H. R. and The Solar Orbiter Team (2013), ‘Solar orbiter: Exploring the Sun-Heliosphere connection’, *Sol. Phys.* **285**, 25 – 70.

Müller, D., St. Cyr, O. C., Zouganelis, I., Gilbert, H. R., Marsden, R., Nieves-Chinchilla, T., Antonucci, E., Auchère, F., Berghmans, D., Horbury, T. S., Howard, R. A., Krucker, S., Maksimovic, M., Owen, C. J., Rochus, P., Rodriguez-Pacheco, J., Romoli, M., Solanki, S. K., Bruno, R., Carlsson, M., Fludra, A., Harra, L., Hassler, D. M., Livi, S., Louarn, P., Peter, H., Schühle, U., Teriaca, L., del Toro Iniesta, J. C., Wimmer-Schweingruber, R. F., Marsch, E., Velli, M., Groof, A. D., Walsh, A. and Williams, D. (2020), ‘The Solar Orbiter mission: science overview’, *Astron. Astrophys.* **642**, A1.

Ness, N. F., Behannon, K. W., Lepping, R. P., Whang, Y. C. and Schatten, K. H. (1974), ‘Magnetic Field Observations near Mercury: Preliminary Results from Mariner 10’, *Science* **185**, 151 – 160.

560 Odstrčil, D. and Pizzo, V. J. (1999a), ‘Three-dimensional propagation of CMEs in a structured solar wind flow: 1. CME launched within the streamer belt’, *104*, 483 – 492.

Odstrčil, D. and Pizzo, V. J. (1999b), ‘Three-dimensional propagation of CMEs in a structured solar wind flow: 2. CME launched adjacent to the streamer belt’, *104*, 493 – 504.

565 Orsini, S., Livi, S., Torkar, K., Barabash, S., Milillo, A., Wurz, P., Di Lellis, A. D., Kallio, E. and the SERENA team (2010), ‘SERENA: A suite of four instruments (ELENA, STROFIO, PICAM and MIPA) on board BepiColombo-MPO for particle detection in the Hermean environment’, *Planet. Space Sci.* **58**, 166 – 181.

570 Orsini, S., Livia, S., Lichtenegger, H., Barabasha, S., Milillo, A., De Angelis, E., Phillips, M., Laky, G., Wieser, M., Olivieri, A., Plainaki, C., Ho, G., Killen, R., Slavin, J., Wurz, P., Berthelier, J.-J., Dandouras, I., Kallio, E., McKenna-Lawlor, S., Szalai, S., Torkar, K., Vaisberg, O., Allegrini, F., Daglis, I., Dong, C., Escoubet, C., Fatemi, S., Fränz, M., Ivanovski, S., Krupp, N., Lammer, H., Leblanc, F., Mangano, V., Mura, A., Nilsson, H., Raines, J., Rispoli, R., Sarantos, M., Smith, H., Szego, K., Aronica, A., Camozzi, F., Di Lellis, A., Fremuth, G., Giner, F., Gurnee, R., Hayes, J., Jeszenszky, H., Tominetti, F., Trantham, B., Balaz, J., Baumjohann, W., Brienza, D., Bührke, U., Bush, M., Cantatore, M., Cibella, S., Colasanti, L., Cremonese, G., Cremonesi, L., D’Alessandro, M., Delcourt, D., Delva, M., Desai, M., Fama, M., Ferris, M., Fischer, H., Gaggero, A., Gamborino, D., Garnier, P., Gibson, W., Goldstein, R., Grande, M., Grishin, V., Haggerty, D., Holmström, M., Horvath, I., Hsieh, K.-C., Jacques, A., Johnson, R., Kazakov, A., Kecskemeti, K., Krüger, H., Kürbisch, C., Lazzarotto, F., Leblanc, F., Leichtfried, M., Leoni, R., Loose, A., Maschietti, D., Massetti, S., Mattioli, F., Miller, G., Moissenko, D., Morbidini, A., Noschese, R., Nuccilli, F., Nunez, C., Paschalidis, N., Persyn, S., Piazza, D., Oja, M., Ryno, J., Schmidt, W., Scheer, J., Shestakov, A., Shuvalov, S., Seki, K., Selci, S., Smith, K., Sordini, R., Svensson, J., Szalai, L., Toublanc, D., Urdiales, C., Varsani, A., Vertolli, N., Wallner, R., Wahlstroem, P., Wilson, P. and Zampieri, S. (2021a), ‘Serena: Particle instrument suite for determining the Sun-Mercury interaction from BepiColombo’, *Space Sci. Rev.* **217**, 11.

575 Orsini, S., Livia, S., Lichtenegger, H., Barabasha, S., Milillo, A., De Angelis, E., Phillips, M., Laky, G., Wieser, M., Olivieri, A., Plainaki, C., Ho, G., Killen, R., Slavin, J., Wurz, P., Berthelier, J.-J., Dandouras, I., Kallio, E., McKenna-Lawlor, S., Szalai, S., Torkar, K., Vaisberg, O., Allegrini, F., Daglis, I., Dong, C., Escoubet, C., Fatemi, S., Fränz, M., Ivanovski, S., Krupp, N., Lammer, H., Leblanc, F., Mangano, V., Mura, A., Nilsson, H., Raines, J., Rispoli, R., Sarantos, M., Smith, H., Szego, K., Aronica, A., Camozzi, F., Di Lellis, A., Fremuth, G., Giner, F., Gurnee, R., Hayes, J., Jeszenszky, H., Tominetti, F., Trantham, B., Balaz, J., Baumjohann, W., Brienza, D., Bührke, U., Bush, M., Cantatore, M., Cibella, S., Colasanti, L., Cremonese, G., Cremonesi, L., D’Alessandro, M., Delcourt, D., Delva, M., Desai, M., Fama, M., Ferris, M., Fischer, H., Gaggero, A., Gamborino, D., Garnier, P., Gibson, W., Goldstein, R., Grande, M., Grishin, V., Haggerty, D., Holmström, M., Horvath, I., Hsieh, K.-C., Jacques, A., Johnson, R., Kazakov, A., Kecskemeti, K., Krüger, H., Kürbisch, C., Lazzarotto, F., Leblanc, F., Leichtfried, M., Leoni, R., Loose, A., Maschietti, D., Massetti, S., Mattioli, F., Miller, G., Moissenko, D., Morbidini, A., Noschese, R., Nuccilli, F., Nunez, C., Paschalidis, N., Persyn, S., Piazza, D., Oja, M., Ryno, J., Schmidt, W., Scheer, J., Shestakov, A., Shuvalov, S., Seki, K., Selci, S., Smith, K., Sordini, R., Svensson, J., Szalai, L., Toublanc, D., Urdiales, C., Varsani, A., Vertolli, N., Wallner, R., Wahlstroem, P., Wilson, P. and Zampieri, S. (2021b), ‘Serena: Particle instrument suite for determining the Sun-Mercury interaction from BepiColombo’, *Space Sci. Rev.* **217**, 11.

580 Orsini, S., Livia, S., Lichtenegger, H., Barabasha, S., Milillo, A., De Angelis, E., Phillips, M., Laky, G., Wieser, M., Olivieri, A., Plainaki, C., Ho, G., Killen, R., Slavin, J., Wurz, P., Berthelier, J.-J., Dandouras, I., Kallio, E., McKenna-Lawlor, S., Szalai, S., Torkar, K., Vaisberg, O., Allegrini, F., Daglis, I., Dong, C., Escoubet, C., Fatemi, S., Fränz, M., Ivanovski, S., Krupp, N., Lammer, H., Leblanc, F., Mangano, V., Mura, A., Nilsson, H., Raines, J., Rispoli, R., Sarantos, M., Smith, H., Szego, K., Aronica, A., Camozzi, F., Di Lellis, A., Fremuth, G., Giner, F., Gurnee, R., Hayes, J., Jeszenszky, H., Tominetti, F., Trantham, B., Balaz, J., Baumjohann, W., Brienza, D., Bührke, U., Bush, M., Cantatore, M., Cibella, S., Colasanti, L., Cremonese, G., Cremonesi, L., D’Alessandro, M., Delcourt, D., Delva, M., Desai, M., Fama, M., Ferris, M., Fischer, H., Gaggero, A., Gamborino, D., Garnier, P., Gibson, W., Goldstein, R., Grande, M., Grishin, V., Haggerty, D., Holmström, M., Horvath, I., Hsieh, K.-C., Jacques, A., Johnson, R., Kazakov, A., Kecskemeti, K., Krüger, H., Kürbisch, C., Lazzarotto, F., Leblanc, F., Leichtfried, M., Leoni, R., Loose, A., Maschietti, D., Massetti, S., Mattioli, F., Miller, G., Moissenko, D., Morbidini, A., Noschese, R., Nuccilli, F., Nunez, C., Paschalidis, N., Persyn, S., Piazza, D., Oja, M., Ryno, J., Schmidt, W., Scheer, J., Shestakov, A., Shuvalov, S., Seki, K., Selci, S., Smith, K., Sordini, R., Svensson, J., Szalai, L., Toublanc, D., Urdiales, C., Varsani, A., Vertolli, N., Wallner, R., Wahlstroem, P., Wilson, P. and Zampieri, S. (2021c), ‘Serena: Particle instrument suite for determining the Sun-Mercury interaction from BepiColombo’, *Space Sci. Rev.* **217**, 11.

585 Orsini, S., Livia, S., Lichtenegger, H., Barabasha, S., Milillo, A., De Angelis, E., Phillips, M., Laky, G., Wieser, M., Olivieri, A., Plainaki, C., Ho, G., Killen, R., Slavin, J., Wurz, P., Berthelier, J.-J., Dandouras, I., Kallio, E., McKenna-Lawlor, S., Szalai, S., Torkar, K., Vaisberg, O., Allegrini, F., Daglis, I., Dong, C., Escoubet, C., Fatemi, S., Fränz, M., Ivanovski, S., Krupp, N., Lammer, H., Leblanc, F., Mangano, V., Mura, A., Nilsson, H., Raines, J., Rispoli, R., Sarantos, M., Smith, H., Szego, K., Aronica, A., Camozzi, F., Di Lellis, A., Fremuth, G., Giner, F., Gurnee, R., Hayes, J., Jeszenszky, H., Tominetti, F., Trantham, B., Balaz, J., Baumjohann, W., Brienza, D., Bührke, U., Bush, M., Cantatore, M., Cibella, S., Colasanti, L., Cremonese, G., Cremonesi, L., D’Alessandro, M., Delcourt, D., Delva, M., Desai, M., Fama, M., Ferris, M., Fischer, H., Gaggero, A., Gamborino, D., Garnier, P., Gibson, W., Goldstein, R., Grande, M., Grishin, V., Haggerty, D., Holmström, M., Horvath, I., Hsieh, K.-C., Jacques, A., Johnson, R., Kazakov, A., Kecskemeti, K., Krüger, H., Kürbisch, C., Lazzarotto, F., Leblanc, F., Leichtfried, M., Leoni, R., Loose, A., Maschietti, D., Massetti, S., Mattioli, F., Miller, G., Moissenko, D., Morbidini, A., Noschese, R., Nuccilli, F., Nunez, C., Paschalidis, N., Persyn, S., Piazza, D., Oja, M., Ryno, J., Schmidt, W., Scheer, J., Shestakov, A., Shuvalov, S., Seki, K., Selci, S., Smith, K., Sordini, R., Svensson, J., Szalai, L., Toublanc, D., Urdiales, C., Varsani, A., Vertolli, N., Wallner, R., Wahlstroem, P., Wilson, P. and Zampieri, S. (2021d), ‘Serena: Particle instrument suite for determining the Sun-Mercury interaction from BepiColombo’, *Space Sci. Rev.* **217**, 11.

590 Orsini, S., Livia, S., Lichtenegger, H., Barabasha, S., Milillo, A., De Angelis, E., Phillips, M., Laky, G., Wieser, M., Olivieri, A., Plainaki, C., Ho, G., Killen, R., Slavin, J., Wurz, P., Berthelier, J.-J., Dandouras, I., Kallio, E., McKenna-Lawlor, S., Szalai, S., Torkar, K., Vaisberg, O., Allegrini, F., Daglis, I., Dong, C., Escoubet, C., Fatemi, S., Fränz, M., Ivanovski, S., Krupp, N., Lammer, H., Leblanc, F., Mangano, V., Mura, A., Nilsson, H., Raines, J., Rispoli, R., Sarantos, M., Smith, H., Szego, K., Aronica, A., Camozzi, F., Di Lellis, A., Fremuth, G., Giner, F., Gurnee, R., Hayes, J., Jeszenszky, H., Tominetti, F., Trantham, B., Balaz, J., Baumjohann, W., Brienza, D., Bührke, U., Bush, M., Cantatore, M., Cibella, S., Colasanti, L., Cremonese, G., Cremonesi, L., D’Alessandro, M., Delcourt, D., Delva, M., Desai, M., Fama, M., Ferris, M., Fischer, H., Gaggero, A., Gamborino, D., Garnier, P., Gibson, W., Goldstein, R., Grande, M., Grishin, V., Haggerty, D., Holmström, M., Horvath, I., Hsieh, K.-C., Jacques, A., Johnson, R., Kazakov, A., Kecskemeti, K., Krüger, H., Kürbisch, C., Lazzarotto, F., Leblanc, F., Leichtfried, M., Leoni, R., Loose, A., Maschietti, D., Massetti, S., Mattioli, F., Miller, G., Moissenko, D., Morbidini, A., Noschese, R., Nuccilli, F., Nunez, C., Paschalidis, N., Persyn, S., Piazza, D., Oja, M., Ryno, J., Schmidt, W., Scheer, J., Shestakov, A., Shuvalov, S., Seki, K., Selci, S., Smith, K., Sordini, R., Svensson, J., Szalai, L., Toublanc, D., Urdiales, C., Varsani, A., Vertolli, N., Wallner, R., Wahlstroem, P., Wilson, P. and Zampieri, S. (2021e), ‘Serena: Particle instrument suite for determining the Sun-Mercury interaction from BepiColombo’, *Space Sci. Rev.* **217**, 11.

595 A., Noschese, R., Nuccilli, F., Nunez, C., Paschalidis, N., Persyn, S., Piazza, D., Oja, M., Ryno, J., Schmidt, W., Scheer, J., Shestakov, A., Shuvalov, S., Seki, K., Selci, S., Smith, K., Sordini, R., Svensson, J., Szalai, L., Toublanc, D., Urdiales, C., Varsani, A., Vertolli, N., Wallner, R., Wahlstroem, P., Wilson, P. and Zampieri, S. (2021b), 'Correction to: SERENA: Particle instrument suite for determining the Sun-Mercury interaction from BepiColombo', *Space Sci. Rev.* **217**, 30.

Phillips, J. L. and McComas, D. J. (1991), 'The magnetosheath and magnetotail of Venus', *Space Sci. Rev.* **55**, 1 – 80.

Pinto, M., Sanchez-Cano, B., Moissl, R., Cardoso, C., Goncalves, P., Assis, P., Vainio, R., Oleynik, P., Lehtolainen, A., Grande, M. and McComas, A., (2021), 'The Bepicolombo Radiation Monitor, BERM', *Space Sci. Rev.* p. Submitted(?).

600 Poh, G., Sun, W., Clink, K. M., Slavin, J. A., Dewey, R. M., Jia, X., Raines, J. M., DiBraccio, G. A. and Espley, J. R. (2020), 'Large-amplitude oscillatory motion of mercury's cross-tail current sheet', *J. Geophys. Res.* **125**, e2020JA027783.

Rong, J. Z., Barabash, S., Stenberg, G., Futaana, Y., Zhang, T. L., Wan, W. X., Wei, Y., Wang, X. D., Chai, L. H. and Zhong, J. (2015), 'The flapping motion of the Venusian magnetotail: Venus Express observations', *J. Geophys. Res.* **120**, 5593 – 5602.

Russell, C. T., Luhmann, J. G., Elphic, R. C. and Scarf, F. L. (1981), 'The distant bow shock and magnetotail of Venus: Magnetic field and 605 plasma wave observations', *Geophys. Res. Lett.* **8**, 843 – 846.

Saito, Y. and et al. (2021), 'Pre-flight calibration and near-earth commissioning results of mercury plasma particle experiment (mppe) onboard mmo (mio)', *Space Sci. Rev.* p. Submitted(?).

Saito, Y., Sauvaud, J. A., Hirahara, M., Barabash, S., Delcourt, D., Takashima, T., Asamura, K. and BepiColombo MMO/MPPE team (2010), 'Scientific objectives and instrumentation of Mercury Plasma Particle Experiment (MPPE) onboard MMO', *Planet. Space Sci.* **58**, 182 – 610 200.

Sánchez-Cano, B., Hall, B. E. S., Lester, M., Mays, M. L., Witasse, O., Ambrosi, R., Andrews, D., Cartacci, M., Cicchetti, A., Holström, M., Imber, S., Kajdič, P., Milan, S. E., Noschese, R., Osdtrcil, D., Opgenoorth, H., Plaut, J., Ramstad, R. and Reyes-Ayala, K. I. (2017), 'Mars plasma system response to solar wind disturbances during solar minimum', *J. Geophys. Res.* **122**, 6611 – 6634.

Saunders, M. A. and Russell, C. T. (1986), 'Avarage dimensino and magnetic structure of the distant Venus magnetotail', *J. Geophys. Res.* 615 **91**, 5589 – 5604.

Schmid, D., Plaschke, F., Narita, Y., Volwerk, M. and Baumjohann, W. (2021), 'Magnetosheath plasma flow model around Mercury', *Ann. Geophys.* p. submitted.

Semkova, J., Koleva, R., Benghin, V., Dachev, T., Matviichuk, Y., Tomov, B., Krastev, K., Maltchev, S., Dimitrov, P., Mitrofanov, I., Malahov, A., Golovin, D., Mokrousov, M., Sanin, A., Litvak, M., Kozyrev, A., Tretyakov, V., Nikiforov, S., Vostrukhin, A., Fedosov, F., Greben- 620 nikova, N., Zelenyi, L., Shurshakov, V. and Drobishev, S. (2018), 'Charged particles radiation measurements with Liulin-MO dosimeter of FREND instrument aboard ExoMars Trace Gas Orbiter during the transit and in high elliptic Mars orbit, ', *Icarus* **303**, 53 – 66.

Sergeev, V., Runov, A., Baumjohann, W., Nakamura, R., Zhang, T. L., Volwerk, M., Balogh, A., Rème, H., Sauvaud, J.-A., André, M. and Klecker, B. (2003), 'Current sheet flapping motion and structure observed by Cluster', *Geophys. Res. Lett.* **30**, 1327.

Shiota, D. and Kataoka, R. (2016), 'Magnetohydrodynamic simulation of interplanetary propagation of multiple coronal mass ejections with 625 internal magnetic flux rope (SUSANOO-CME)', *Space Weather* **14**, 56 – 75.

Shiota, D., Kataoka, R., Miyoshi, Y., Hara, T., Tao, C., Masunaga, K., Futaana, Y. and Terada, N. (2014), 'Inner heliosphere MHD modeling system applicable to space weather forecasting for the other planets', *Space Weather* **12**, 187 – 204.

Slavin, J. A., Intriligator, D. S. and Smith, E. J., 'Pioneer Venus Orbiter Magnetic Field and Plasma Observations in the Venus Magnetotail', *J. Geophys. Res.* **94**, 2383 – 2398.

630 Spreiter, J. R. and Stahara, S. S. (1994), 'Gasdynamic and magnetohydrodynamic modeling of the magnetosheath: a tutorial', *Adv. Space Res.* **14**, 5 – 19.

Spreiter, J., Summers, A. and Alksne, A. (1966), 'Hydromagnetic flow around the magnetosphere', *Planet. Space Sci.* **14**, 223 – 253.

Svedhem, H., Titov, D. V., McCoy, D., Lebreton, J.-P., Barabash, S., Bertaux, J.-L., Drossart, P., Formisano, V., Häusler, B., Koralev, O., Markiewicz, W. J., Nevejans, D., Pätzold, M., Piccioni, G., Zhang, T. L., Taylor, F. W., Lellouch, E., Koschny, D., Witasse, O., Eggel, H., Warhaut, M., Accomazzo, A., Rodriguez-Canabal, J., Fabrega, J., Schirrmann, T., Clochet, A. and Coradini, M. (2007), 'Venus Express: The first European mission to Venus', *Planet. Space Sci.* **55**, 1636 – 1652.

Verigin, M. I., Gringauz K. I., Gombosi, T., Breus, T. K., Bezrukikh, V. V., Premizov, A. P. and Volkov, G. I. (1978), 'Plasma near Venus from the Venera 9 and 10 Wide-Angle analyzer data', *J. Geophys. Res.* **83**, 3721 – 3728.

Volwerk, M., Delva, M., Futaana, Y., Retinò, A., Vörös, Z., Zhang, T. L., Baumjohann, W. and Barabash, S. (2009), 'Substorm activity in Venus's magnetotail', *Ann. Geophys.* **27**, 2321 – 2330.

640 Volwerk, M., Delva, M., Futaana, Y., Retinò, A., Vörös, Z., Zhang, T. L., Baumjohann, W. and Barabash, S. (2010), 'Corrigendum to "substorm activity in Venus's magnetotail" published in Ann. Geophys., 27, 2321 - 2330, doi:10.5194/angeo-27-2321-2009, 2009', *Ann. Geophys.* **28**, 1877 – 1878.

Volwerk, M., Horbury, T. S., Woodham, L. D., Bale, S. D., Simon Wedlund, C., Schmid, D., Allan, R. C., Angelini, V., Baumjohann, W., Berger, L., Edberg, N. J. T., Evans, V., Hadid, L. Z., Ho, G. C., Khotyaintsev, Y. V., Magnes, W., Maksimovic, M., O'Brien, H., Steller, M. B., Rodriguez-Pacheco, J. and Wimmer-Scheingruber, R. F. (2021), 'Solar Orbiter's first Venus flyby: MAG observations of structures and waves associated with the induced Venusian magnetosphere', *Astron. Astrophys.* p. submitted.

Volwerk, M., Schmid, D., Tsurutani, B. T., Delva, M., Plaschke, F., Narita, Y., Zhang, T. L. and Glassmeier, K.-H. (2016), 'Mirror mode waves in Venus's magnetosheath: solar minimum vs. solar maximum', *Ann. Geophys.* **34**, 1099 – 1108.

650 Volwerk, M., Zhang, T. L., Delva, M., Vörös, Z., Baumjohann, W. and Glassmeier, K.-H. (2008a), 'First identification of mirror mode waves in venus' magnetosheath?', *Geophys. Res. Lett.* **35**, L12204.

Volwerk, M., Zhang, T. L., Delva, M., Vörös, Z., Baumjohann, W. and Glassmeier, K.-H. (2008b), 'Mirror-mode-like structures in venus' induced magnetosphere', *J. Geophys. Res.* **113**, E00B16.

Vörös, Z., Zhang, T. L., Leubner, M. P., Volwerk, M., Delva, M. and Baumjohann, W. (2008), 'Intermittent turbulence, noisy fluctuations, 655 and wavy structures in the Venusian magnetosheath and wake', *J. Geophys. Res.* **113**, E00B21.

Vörös, Z., Zhang, T., Leubner, M. P., Volwerk, M., Delva, M., Baumjohann, W. and Kudela, K. (2008), 'Magnetic fluctuations and turbulence in the Venus magnetosheath and wake', *Geophys. Res. Lett.* **35**, L11102.

Witasse, O., Sánchez-Cano, B., Mays, M. L., Kajdic, P., Opgenoorth, H., Elliott, H. A., Richardson, I. G., Zouganelis, I., Zender, J., Wimmer-Scheingruber, R. F., Turc, L., Taylor, M. G. G. T., Roussos, E., Rouillard, A., Richter, I., Richardson, J. D., Ramstad, R., Provan, G., 660 Posner, A., Plaut, J. J., Odstrcil, D., Nilsson, H., Niemenen, P., Milan, S. E., Mandt, K., Lohf, H., Lester, M., Lebreton, J.-P., Kuulkers, E., Krupp, N., Koenders, C., James, M. K., Intzakara, D., Holmstrom, M., Hassler, D. M., Hall, B. E. S., Guo, J., Goldstein, R., Goetz, C., Glassmeier, K. H., Génot, V., Evans, H., Espley, J., Edberg, N. J. T., Dougherty, M., Cowley, S. W. H., Burch, J., Behar, E., Barabash, S., Andrews, D. J. and Altobelli, N. (2017), 'Interplanetary coronal mass ejection observed at STEREO-A, Mars, comet 67P/Churyumov-Gerasimenko, Saturn, and New Horizons en route to Pluto: Comparison of its Forbush decreases at 1.4, 3.1, and 9.9 AU', *J. Geophys. Res.* **122**, 7865 – 7890.

Zhang, T. L., Baumjohann, W., Delva, M., Auster, H.-U., Balogh, A., Russell, C. T., Barabash, S., Balikhin, M., Berghofer, G., Biernat, H. K., Lammer, H., Lichtenegger, H., Magnes, W., Nakamura, R., Penz, T., Schwingenschuh, K., Vörös, Z., Zambelli, W., Fornacon,

K.-H., Glassmeier, K.-H., Richter, I., Carr, C., Kudela, K., Shi, J. K., Zhao, H., Motschmann, U. and Lebreton, J.-P. (2006), 'Magnetic field investigation of the venus plasma environment: Expected new results', *Planet. Space Sci.* **54**, 1336 – 1343.

670 Zhang, T. L., Delva, M., Baumjohann, W., Volwerk, M., Russell, C. T., Barabash, S., Balakin, M., Pope, S., Glassmeier, K.-H., Wang, C. and Kudela, K. (2008), 'Initial Venus Express magnetic field observations of the magnetic barrier at solar minimum', *Planet. Space Sci.* **56**, 790 – 795.

Zhang, T. L., Delva, M., Baumjohann, W., Volwerk, M., Russell, C. T., Wei, H. Y., Wang, C., Balikhin, M., Barabash, S., Auster, H.-U. and Kudela, K. (2008), 'Induced magnetosphere and its outer boundary at Venus', *J. Geophys. Res.* **113**, E00B20.

675 Zhang, T. L., Lu, Q., Baumjohann, W., Russell, C. T., Fedorov, A., Barabash, S., Coates, A. J., Du, A. M., Cao, J. B., Nakamura, R., Teh, W. L., Wang, R. S., Dou, X. K., Wang, X., Glassmeier, K. H., Auster, H. U. and Balakin, M. (2010), 'Magnetic reconnection in the near Venusian magnetotail', *Science* **336**, 567 – 570.

Zhang, T. L., Nakamura, R., Volwerk, M., Runov, A., Baumjohann, W., Eichelberger, H. U., Carr, C., Balogh, A., Sergeev, V., Shi, J. K. and Fornaçon, K.-H. (2005), 'Double Star/Cluster observation of neutral sheet oscillations on August 5, 2004', *Ann. Geophys.* **23**, 2909 – 680 2914.